CrossMark

The effect of particle shape on mixing in a high shear mixer

Matthew D. Sinnott[1] · Paul W. Cleary[1]

Abstract Discrete element method modelling is used to study the effect of particle shape on the flow dynamics and mixing in a high shear mixer. The blade generates strong flow over its top surface while compacting and pushing forward particles that are directly in front of the blade. A complex three dimensional flow is established with vertical and radial flow components that are shape dependent and which control the nature of the mixing. Mixing was found to be fast in the azimuthal direction, of intermediate speed in the vertical direction and comparatively slow in the radial mixing. Diffusive mixing is characterised using the granular temperature which shows that the regions of higher granular temperature are larger for round particles than non-round ones leading to stronger diffusive mixing. The spatial distribution of the convective component of mixing is identified using novel calculation of shear strain rate. This size and shape of the high shear region is found to be only slightly sensitive to the particle shape indicating that the convective mixing is relatively independent of shape, except in the middle of the mixer. The blockiness of the particles has the strongest impact on flow and mixing while the mixing has only a weak dependence on the particle aspect ratio.

Keywords Granular mixing · Particle shape · DEM · High shear mixer · Super-quadric

✉ Paul W. Cleary
paul.cleary@csiro.au

[1] CSIRO Digital Productivity Flagship, Private Bag 10, Clayton South, Vic 3168, Australia

1 Introduction

The mixing of granular systems such as powders is a fundamental operation, and is important for a range of industries including pharmaceuticals and food processing. The quality of the product depends on the degree of mixing of its constituent materials. The homogeneity of the final mixture relies, in turn, on the nature of the mixing procedure. Usually there is an equilibrium limit where further mixing is balanced by segregation and other de-mixing processes [43]. This mixing limit and the rate at which it can be reached typically both depend on the design and operation of the mixing device. Limited progress has been made in improving mixer design because of the difficulty in measuring the progress of mixing and limitations in understanding of the interactions between mixer geometry and the nature of the granular material [44]. Numerical models can provide a means for studying such systems by providing detailed quantitative information on the progress of mixing (for example, [42]) and how this varies with design, manner of operation and the properties of granular material.

There are many challenges in developing computational models for studying granular mixing in commercial devices. Production-scale rotary batch mixers typically have capacities of hundreds of litres (and can range up to 20,000 l) filled with wet/cohesive, non-spherical particles of sizes down to tens of microns. Scale-up from laboratory designs is also still poorly understood for the majority of mixing devices. Ding et al. [20] describe scaling relationships for rotary drums, but these are not typically available for other mixing devices.

In order to simulate mixing of granular materials it is necessary to include the grain scale physics and to predict the effects of collisions. The discrete element method (DEM) is now a widely used tool to simulate particle flows in industrial

applications (see [12,14,21,25,26] and [55] for examples). DEM models of granular mixing have so far been predominantly for small-scale laboratory mixers because of the high computational expense for simulating very large industrial mixers. In this modelling, the particles have typically been represented as spherical (for example [3]) and quite often as dry and non-cohesive. It has been shown that mixing rates for dry, free flowing materials in rotating drums are independent of rotational speed in the range 6–14 rpm whereas cohesive materials in the same range are not [51]. Chauduri et al. [8] showed that for cohesive materials in tumbling mixers, a higher rotational speed results in more rapid mixing for 12.5–30 rpm. Liu et al. [36] found that mixing performance in tumbling devices degraded with the addition of cohesive forces. Both Sarkar [47] and Dubey [22] predicted only very subtle differences in mixing performance for different cohesion levels where any differences were only observed at low impeller speeds. Radl et al. [45] observed that for a bladed mixer, moisture content affected the spatial distribution of mixing intensity resulting in greater vertical velocity fluctuations and larger heap size near the blade leading to higher mixing rates for wet material. Experimental measurements of cohesive powders in a tumbling blender [2] using NIR spectroscopy have shown that cohesive mixing degrades for high fill levels and slow blending speeds.

High shear mixers are a specific class of stirred mixer that uses a high-speed impeller to mix the granular material [16]. Industrial versions of these typically run at 100–1000 rpm depending on mixer size to give tip speeds of 10 m/s or greater [29]. At these speeds, the impeller fluidizes the outer portions of the bed, throwing the particulates into the air. However most numerical studies to date Stewart et al. [50], 2003; [7,48,57,58] have only considered simple rectangular paddle impeller geometries at much lower speeds (<1.5 m/s tip speed) which involve impeller interactions with a bed that remains densely packed. These studies have all used DEM models, but assumed spherical shapes for the particles with small values of rolling friction to attempt to account for mild departures from sphericity.

Stewart et al. [49,50] validated their DEM model against PEPT measurements of a mixer with 2–2.4 mm glass beads. They studied heap formation in front of the paddle tip, mixing recirculation zones inside the heap, and flow over the paddle, as well as the effect of rolling and sliding friction on their predictions. Zhou et al. [57] used the same mixer model to investigate flow and segregation in binary mixtures of alternatively different size and different density materials. They found that the upward force on the particles flowing over the paddle was the mechanism responsible for segregation effects. They later performed a more comprehensive study [58] of the effect of rolling and sliding friction on flow, bed structure, mixing performance and inter-particle forces. They showed that mixing kinetics were enhanced for low friction

materials. However for materials with higher sliding friction and higher rolling resistance (as a proxy for non-sphericity) they found that the bed dilated causing increased bed porosity, stronger recirculation zones and higher mixer torque.

Kuo at al. [30] investigated flow in such a mixer using paddle and disc impellers with a speed of 100 rpm (corresponding to a tip speed of 0.7 m/s). However, the model predicted more violent agitation of the bed when using the paddle than was observed in the PEPT measurements. Sato et al. [48] demonstrated the use of impeller torque as a measure of the total powder kinetic energy in the mixer. Chandratilleke et al. [7] investigated flow and mixing performance as a function of impeller speed from 2–100 rpm (with tip speeds up to 1.3 m/s). They found that the significance of the recirculation zones in the heap identified by earlier researchers diminishes with increasing speed and that larger voids form behind the paddle. The mixing rate was shown to increase with blade speed so that less time was required to reach steady state. However, the amount of mixing per revolution was found to decrease with increasing speed until about 50 rpm after which it remained constant. Cleary and Sinnott [16] also used DEM to examine mixing in high shear mixers with paddle and disc impellers.

Very few DEM studies have been performed of high shear mixers at realistic impeller speeds. Terashita et al. [53] used a DEM model of a multi-bladed impeller with tip speeds of 2 and 4 m/s mixing a bed of 3 mm spheres to investigate segregation effects in a binary mixture of different density materials. They found that segregation effects which degrade mixture quality can be managed with an appropriate choice of impeller speed and duration of mixing. At impeller speeds where fluidisation of the bed occurs, the effect of air drag on particulates may become important. Since drag forces depend on particle shape because of the variation in projected surface area in the direction of motion, so mixing and segregation may exhibit additional shape dependence.

Usually citing computational expense, most researchers using DEM to simulate mixing processes in three dimensions use spherical particles. However, particle shape can vary substantially both between different types of particles and between specific particles from the same population. It is also known to be of critical importance in obtaining quantitative accuracy for the prediction of mixing in rotating drums [9,11,24,31]. The use of round particles to represent cubic salt particles was shown to lead to the wrong flow pattern being predicted by the DEM model and consequent errors in mixing rates that were at best quantitatively wrong by more than an order of magnitude. Cleary and Metcalfe [11] demonstrated that when the particle shape was better represented (as super-quadrics) that the correct flow pattern was predicted and mixing rates were then of the correct order. The key reason for this problem is that round particles have relatively low resistance to shear compared to more angular or

blocky particles [14] and therefore flow too easily leading to deformation in regions that should not be deforming. Laurent and Cleary [33] used DEM to investigate mixing flow in a ploughshare mixer, representing the particles as spheres and found by comparison to PEPT that the predictions of the free surface angles were too low. Cleary [15] used a super-quadric representation to closely match the shapes of the rice particles and obtained higher surface angles that were in better agreement with the experiments. The mixing rates were also found to change in response to the inclusion of the particle shape. A brief review of different particle shape models used for mixing applications is given in [5]. Commonly, particle clusters of overlapping spheres have been used to represent more complex particle shapes but these increase the size of the overall computation by increasing the number of particles in the simulation [23,27,38,56].

Adequate representation of shape in a DEM model can therefore be a major problem for correctly predicting mixing rates, where the flow regime and mixing patterns for realistic particle assemblies can depart significantly from those of spheres. The angularity and aspect ratios are important parameters for characterising the shape of particles. Both contribute to particles having higher coordination numbers and influence packing density [19]. They also strongly influence the ability to shear the material by creating more complicated interlocking of the microstructure [13]. The shear strength of a granular material can be characterised by the angle of repose. Debroux and Cleary [18] showed in two dimensions how the different shape attributes affect the angles of repose and failure of granular materials. Mead and Cleary [39] recently extended this analysis to three dimensions. Rolling friction is often applied [1,28,35,36,46,49,50] to modify the flow dynamics by introducing additional numerical resistance to particle rotations in order to mimic the flow behaviour of particles of more complex shape. However this approach is unable to correctly capture key aspects of a granular microstructure of non-spherical particles such as packing density and the degree of dilation of a granular bed in regions of high shear. Understanding the critical role that shape plays in determining packing efficiency, strength of a microstructure, flowability and segregation is important for predicting mixer performance for a given granular material.

The aim of this paper is to investigate the effect of particle shape on mixing in a high shear mixer. We use the same mixer geometry from [30] which was also used in [16]. Mixing in radial, circumferential and axial directions are studied by sub-dividing particles into distinct spatial regions (such as quadrants, annuli and horizontal strata) and following the evolution of these different coloured structures. This is a technique originally used to quantify mixing in laboratory experiments [40,41] but also applied successfully to assessing a range of mixers using DEM [16]. Granular temperature is used to help understand diffusive mixing. A new approach

for characterizing the convective mixing by calculating measures of the shear strain in the bed are presented and used for the high shear mixer. The investigation is performed in three stages to explore different aspects of the particle shape on the mixing dynamics and bed structure. These are a:

- matched comparison between spheres and non-round particles;
- parametric investigation of the effect of varying the angularity of the particles; and
- parametric investigation of the effect of particle aspect ratio using plate and cubic particles.

The effects of each aspect of the particle shape on mixing and flow are determined.

2 Numerical model and measurement of mixing

2.1 Discrete element method

The DEM is a particle-based technique. The general DEM methodology and its variants are well established [4]. Each particle in the flow is tracked and all collisions between particles and between particles and boundaries are modelled. The contact force law used here is a linear spring-dashpot model where particles are allowed to overlap. The maximum overlap, Δx, is fixed by the stiffness of the spring in the normal direction, k_n, which provides a repulsive force. The dashpot contributes the inelastic component of the collision. Its damping coefficient, C_n, determines the effective coefficient of restitution for the material properties of the granular media. The spring and dashpot together define the normal force:

$$F_n = -k_n \, \Delta x + C_n v_n, \tag{1}$$

and the tangential force is:

$$F_t = \min \left\{ \mu F_n, \sum k_t v_t \Delta t + C_t v_t \right\}, \tag{2}$$

where v_n and v_t are the normal and tangential velocities in the collision frame and μ is the coefficient of friction. All the contact parameters are global values and are not scaled by either contact area or particle size (which typically occur for models using Hertzian springs, see [54]). No rolling friction is used as this is very small for real particles and having directed resolved the particle shape using a geometric representation there is no numerical requirement to include an artificial torsional resistance via a rolling friction with unphysically large rolling friction coefficients.

The code used for these simulations has previously been used to model many industrial granular flows (see [12,14] and [10] for details and examples).

In this work, the non-round particle shapes are represented as super-quadrics (SQs) (see [12] for details). Super-quadrics are described by

$$\left(\frac{x}{a}\right)^m + \left(\frac{y}{b}\right)^m + \left(\frac{z}{c}\right)^m = 1. \tag{3}$$

The resultant particles are somewhere between an ellipsoid and a rectangular box with the angularity/smoothness of the corners controlled by the choice of m (with $m = 2$ being ellipsoidal and large m being a brick) and the aspect ratios being controlled by the ratios of the semi-major axes (b/a and c/a). In changing from a spherical particle representation to a super-quadric one increases the computational cost in three ways

1. The cost of each distance calculation between each pair of particles and the determination of the closest points on their surfaces increases
2. The number of near-neighbours increases particularly for higher aspect ratios. Since the basic cost of the DEM algorithm lies in looping over the number of such neighbour pairs then this increases the number of such operations
3. With spherical particles there are often savings to be made by not performing calculations such as those relating to the orientation of the particles. These savings are relatively small and cannot be made for non-round particles.

The overall cost of the inclusion of shape using this approach is very problem dependent with some applications having little extra cost but in extreme cases of dense flows with very high aspect ratios (such as 10:1) the cost can be as high as a factor of ten. Typically the cost tends to be in the range of 2–3 times. For this mixing application the cost difference was about a factor of 3–4 times more expensive for the SQ simulations.

2.2 Characterising mixing state and its time evolution

A method for predicting mixing and segregation in granular systems has previously been described [9]. The method is flexible and can be used with both continuous and discrete particle distributions. A three dimensional grid is constructed over the particles. Local averages of a selected property (e.g. mass, density, diameter, colour) are calculated using all particles in the region centered at each grid point. These local averages then define a probability distribution for the chosen property across the granular system. The mean, standard deviation, and coefficient of variation, η, (defined as mean divided by standard deviation) are calculated for the entire distribution at each time. Theoretical ideal limits are calculated for the coefficient of variation for the fully segregated and fully mixed states, η_s and η_r respectively. This allows η

to be normalised and provide a single mixing measure in the range of 0–1. In practice the diffusion inherent in the calculation of the mixing measure means that even for perfectly mixed particles the mixing measure is typically larger than the perfectly mixed measure. We therefore use the value of the mixing measure after steady state flow has been achieved as the lower bound of the mixing. This ensures that the normalised mixing measure always starts from zero. Since this quantity evolves with time (reflecting mixing and segregation processes in the bed) it is not only a good indicator of the quality of the mixture but also a natural measure of the mixing rate. This mixing/segregation measurement process is described in more detail in Cleary et al. [9] and has been used extensively in [16]. It is also closely related to the Lacey mixing index [32].

The statistical accuracy of the local averages depends on the number of particles included within each cell which is controlled by the ratio of the particle to cell size. If this ratio is too small then the local averages are very variable and the histogram of averages has significant noise. If however, the ratio is too large then there is significant numerical diffusion in the estimation process and local areas of greater or less than average mixing are not captured in the overall distribution and the particle state can be assessed as being more mixed than is actually the case. Here we use cells that are 2.5 minimum particle diameters across each cell edge. This means that in 3D there are typically 30–50 particles used in the calculation of the local averages. The expected standard deviation of the variability of the local means is 0.45 of these means. Therefore the estimate of the local mean is, to a 95 % confidence level, within $\pm 1.35 \times$ of the mean. This is sufficiently accurate for the current purpose and balances the need to have good local estimates of the mean with the need to have sufficient independent data points to accurately characterise the distribution of local means.

2.3 Average flow field, granular temperature and shear rates

In order to better understand the three dimensional flow field and key aspects of the mixing such as where diffusion and convective contributions arise, it is useful to calculate a temporally averaged representation of the flow in the frame that is co-rotating with the mixing blade. This is done by using a grid and then calculating the average of flow quantities based on their values for particles in each cell of the grid.

The diffusion processes occurring within a granular flow vary with the granular temperature which is a measure of the magnitude of the velocity fluctuations [6]. This is the trace of the streaming stress tensor. The definitions of both, and the manner of calculation of the granular temperature using an averaging grid, are given in [13]. It has proven to be a useful concept in describing collision intensity and has been used to

identify strong regions of grinding in tower mills [52]. Here we use the granular temperature as a way of quantifying the diffusive component of mixing and identifying which parts of the flow are responsible for this.

Relating granular temperature to diffusive mixing is well established and has been used by other authors to investigate mixing and segregation effects. Conway et al. [17] investigated the relationship between size segregation effects and temperature gradients in a bladed mixer. They found that their observed segregation patterns were partially explained by granular temperature variations. Lemieux et al. [34] compared mixing behavior in tumbling V-blenders and bin blenders and found that varying rotation speed and fill level significantly affected granular temperatures in the V-blenders, but showed almost no effect for bin blenders. Remy et al. [46] observed that for a stirred mixer increasing particle friction level resulted in increased granular temperatures whereas changing from an obtuse to an acute blade pitch angle reduced them. Lu and Hsiau [37] showed that the apparent diffusion coefficient for a shear cell was linearly dependent to the square root of the transverse temperatures across the cell in a region where the granular material exhibited fluid-like behavior. Radl et al. [45] used granular temperature to investigate cohesive granular mixing in a stirred mixer. They found that for wet materials, that mean velocity fluctuations increased but with a lower variance of velocities resulting in improved diffusive mixing over dry materials.

Convective mixing (sometimes considered as convective-shear mixing) relies on the stretching of the granular material. This behaviour can be evaluated by calculating the strain rate tensor at each point of the grid using the average velocity, v. This is:

$$E_{ij} = \frac{1}{2} \left(\partial_i v_j + \partial_j v_i \right) \tag{4}$$
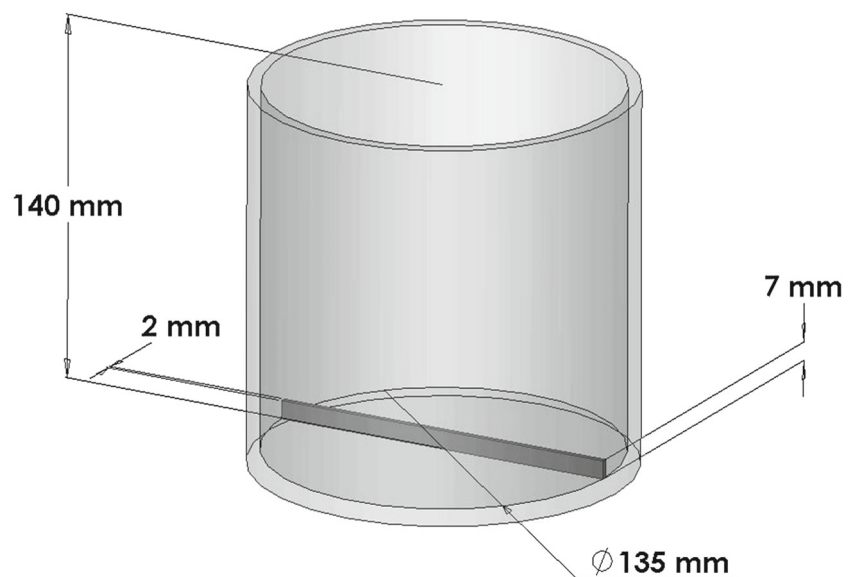
The trace of this matrix measures the dilation or contraction of the granular material. In areas with high shear, particularly for non-round particles, the microstructure necessarily must dilate. In other regions the grains are able to settle and pack better leading to contraction. This is a useful quantity for identifying such dilating and compacting regions. The off-diagonal elements of this matrix are the shear rates in each direction. The matrix is not necessarily symmetric as coupled stresses in granular materials can break the symmetry that is usual in fluids. A simple scalar measure of the shear rate can be obtained by summing the magnitudes of all the off-diagonal elements. This approach is used in this paper to identify high shear regions where convective mixing is strong.

The combination of the granular temperature, dilation rate and shear rate allow us to analyse the spatial variation of the key mechanisms that occur in the mixing flow and to determine their relative importance in different locations relative to the mixing blade.

3 High shear mixer configuration

Following the mixer geometry used in [30], the high shear mixer used for these studies consists of a vertical cylindrical shell of diameter 135 mm with a horizontal floor at the bottom. A rectangular blade impeller is used to perform the mixing. It is 135 mm long in the horizontal direction, 7 mm high in the vertical direction and 2 mm thick. The rotation axis of the impeller is at its center and this is located at the center of the floor of the shell. The ends of the impeller just touch the cylindrical sides of the mixer and there is no clearance between the impeller and the floor. The configuration is shown in Fig. 1. The impeller rotates counter-clockwise with a rotation rate of 100 rpm giving the impeller a tip speed of

Fig. 1 Diagram of mixer geometry showing the cylindrical mixer bowl and blade impeller

Table 1 Particle shape information for the comparison of spherical particle behaviour to a broad mixture of non-round particle shapes

	Spheres	Super-quadric mixture
Angularity	2.0	2.5–6.0
Aspect ratio	1.0	0.7–1.0

Table 2 Particle shapes used in the study of the effect of angularity on mixing

	Case 1	Case 2	Case 3	Case 4
Angularity (Shape factor)	3	4	5	6
Aspect ratio	0.7	0.7	0.7	0.7

Table 3 Particle shapes used in the study of the effect of aspect ratio on mixing

	Case 5	Case 2	Case 6	Case 7
Angularity (Shape factor)	4	4	4	4
Aspect ratio	0.5	0.7	0.85	1.0

0.71 m/s. The mixer has been used in previously reported DEM studies using spherical particles [16].

Three sets of particles were used for the three components of the investigation. These are summarised in Tables 1, 2, 3. In the first part of the study (Table 1) a broad mixture of shapes is used with the angularity distributed uniformly between 2.5 (nearly round) to 6.0 (quite angular with fairly sharp corners) and the aspect ratios were uniformly distributed in the range 0.7–1.0 for both intermediate and minor axes of the particles. For the second and third parts of the study the particle shape was the same for all particles in the same simulation and only one shape attribute was then varied at a time. For the exploration of the angularity (Table 2) the aspect ratio was 0.7 so the particles varied from moderate aspect ratio ellipsoids to equivalent aspect ratio bricks. For the exploration of the aspect ratio (Table 3) the angularity was 4.0 giving moderately blocky shapes while one aspect ratio was varied from equi-axed (giving a cubical particle) to 0.5 (for the minor axis relative to the long axis). This produces particle shapes that vary from plate-like to cubic. Examples of the super-quadric shaped particles used in this study are shown in Fig. 2, with β_{xy} being the aspect ratio between the intermediate and longest axis lengths (calculated in the canonical frame of the particles in which the particles are show) and β_{xz} being the aspect ratio between the shortest and longest axis lengths.

Spherical particle diameters ranged from 1.45 to 1.55 mm to prevent numerical crystallisation effects. The super-quadric particle sizes were chosen so that the spherical and non-spherical grains had the same volume and so the super-quadric particles have the same spherical equivalent diameter. This incidentally means that the numbers of parti-

cles in the spherical and non-spherical simulation cases are the same. A particle density of 2, 500 kg/m^3 was used for all cases. We believe that this is the fairest way to construct particle sets that differ in shape allowing shape influence to be analysed without incidentally creating size distribution variations. The question of how best to create sets of particles with different shape but the same "real" size is far from being answered. Shape and size are inherently linked and size is also strongly influenced by the way in which the particles sizes are measured. Some processes such as screening or sieving tend to be controlled by the intermediate semi-major axis length whereas flow through apertures tends to be more influenced by the largest semi-major axis. For current purposes using the same equivalent spherical volume distribution provides a solid basis for comparison of different shape cases whilst minimising unintended size distribution changes which can strongly affect mixing and segregation processes.

The particle-particle and particle-boundary coefficient of restitution was chosen to be 0.9 representing a reasonably elastic material such as the commonly experimentally used glass ballotini. Stewart et al. [49] found that the structure of particle flows was relatively insensitive to coefficients of friction in the range 0.3–0.5 for DEM simulations of the same type of high shear mixer. A representative dynamic coefficient of friction of 0.4 was therefore chosen for both particle-particle and particle-boundary interactions. These material parameters correspond to those of real materials of the type that would be blended in such a mixer.
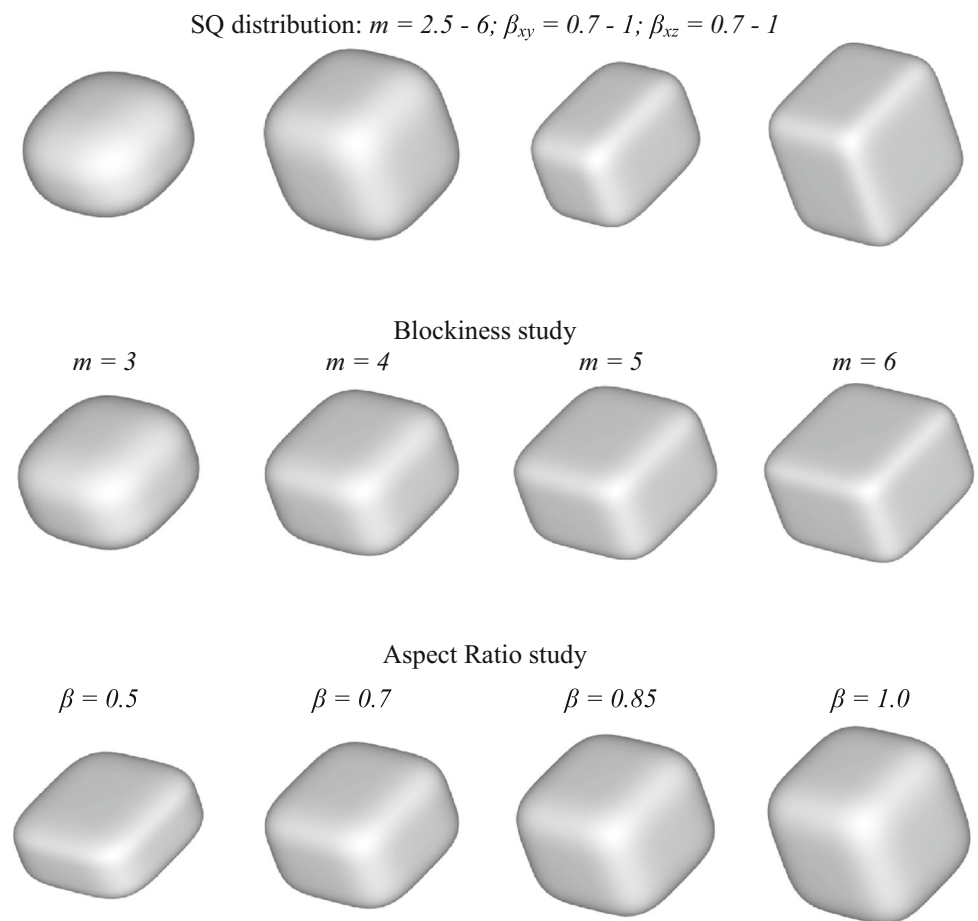
The spring constants are numerical parameters that control the amount of numerical deformation of the particles and also the computational cost via its strong influence on the integration timestep, Here we was a normal spring stiffness $k_n = 100$ N/m which gives an average overlap of 0.7 % of the particle diameter which is sufficient to ensure than the solution is not sensitive to the choice of stiffness. The tangential stiffness used is half the normal stiffness.

For each simulation, the mixer was filled with sufficient particles to give a bed depth of H = 15 mm (which is twice the blade height). This gave a total bed mass of 0.26 kg for each simulation which corresponds to a small number of roughly 60,000 particles. For the assessment of mixing the simulations were run until a statistically steady state flow was achieved. The particles were then coloured using three different schemes,

(1) quadrants,
(2) annular bands, and
(3) vertical strata.

For each colour scheme, four colours were used. The locations of the transitions between colours in each scheme were chosen so that there are equal numbers of particles in each

Fig. 2 Examples of super-quadric shaped particles used in these simulations

SQ distribution: *m = 2.5 - 6; β_{xy} = 0.7 - 1; β_{xz} = 0.7 - 1*

Blockiness study

m = 3   *m = 4*   *m = 5*   *m = 6*

Aspect Ratio study

β = 0.5   *β = 0.7*   *β = 0.85*   *β = 1.0*

colour group for each colour scheme. This means for example that for the annular band scheme the bands differ in width as a result of the changing radius range for each band. As one moves away from the center the circumference of the boundaries of each band become larger and so the bands become thinner so that each band contains the same volume of particles. This also means that for the vertical strata scheme the top strata covers a greater range of vertical height because the free surface is heaped around the locations of the mixing blade. The initial equilibrium colour states of the spherical particle case are shown in Fig. 3. The free surface has two mounds located roughly above the location of the blade with reasonably deep depressions in between. These increase in height with increasing radius due to the increasing blade speed with radius. The top of the blade is just visible in the center of the mixer.

A cylindrical grid is used for the calculation of the average flow field. Its center and axis are aligned with the center and rotation axis of the blade and its diameter corresponds to the diameter of the inner surface of the mixer shell. It has 25 cells in the radial direction, 130 in the azimuthal direction and 40 in the vertical direction.

4 Comparison of spherical and non-spherical cases

4.1 Structure of the flow

It has previously been shown [16] that particle shape can strongly affect the mixing in a high shear mixer. This comparison is interesting and relevant here because the spherical case represents the asymptotic limit of the shape attributes and is the most extreme shape at one end of the shape distribution. To better understand the relative mixing performance of these two cases, we first explore the structure of the equilibrium flow field for both spherical and non-round particles and then relate these to the observed mixing in the three directions (circumferential, radial and vertical).

Figure 4 shows the equilibrium bed coloured by different components of velocity for the mixture of super-quadric shaped particles. The peaks of the raised particle piles which are driven by the motion of the blade trail the blade by around $2° - 3°$. In the regions away from the piles above the blade, the particle speeds are low and the bed is fairly quiescent. But in the pile regions there is significant motion and it has clear structure. The blade is rotating in a counter-clockwise direction so the half blade in the top of each picture is moving
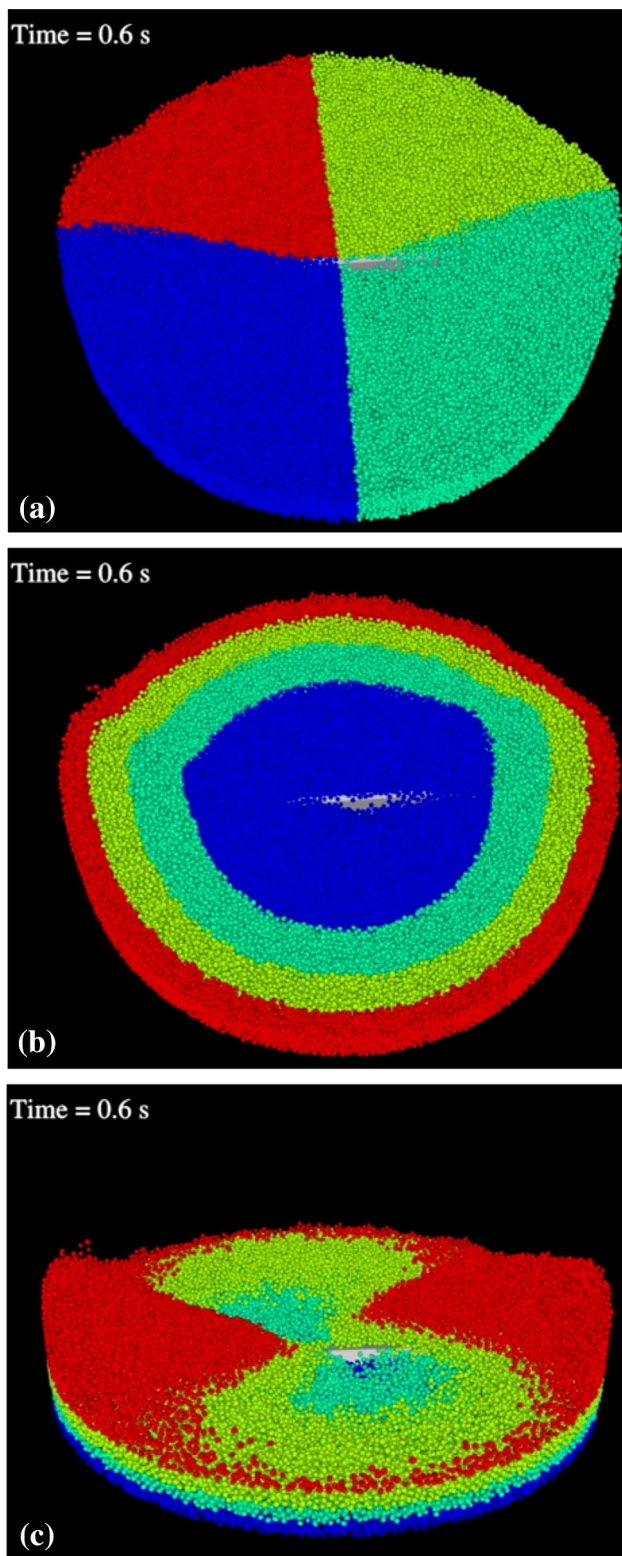
Fig. 3 Bed state once flow has reached equilibrium and particles are coloured in groups according to their positions at that time, **a** quadrants, **b** annuli, and **c** horizontal strata

to the left and the half blade at the bottom is moving to the right. The high azimuthal velocity of the particles in the pile (all red) means that the pile is predominantly moving with the motion of the blade. The speed also increases radially (as a result of the radial increase of the blade speed) and the width of the fast moving pile becomes wider (extends over a progressively larger azimuthal angle range). The pile motion is not a rigid body rotation though as the particles in front of the approaching blade move radially outwards and upwards and particles behind the blade move radially inwards and down towards the main bed surface. When all the velocity components are combined to give the speed, a complex distribution (see Fig. 4d) with a high speed wedge of material both in front of and behind the blade are observed.

Figure 5 shows the corresponding bed surface and velocity distributions for spherical particles. There are strong similarities in the flow behaviour to that of the non-round material shown in Fig. 4. The general area of high speed radial flow is very similar in shape but the peak speeds are higher and the red area is more contiguous and solid. In contrast, there is very little difference in the inward radial flow (blue coloured particles). For the azimuthal velocities, the high speed pile moves more quickly for the spherical particles while the majority of the bed away from the blade moves more slowly (with much of the bed now a dark blue rather than the mid-blue found for the non-round particles). This reflects greater localization of the blade effect for spherical particles which shear more easily and so the blade disturbance is transmitted less effectively and less of the bed is agitated at any time. The difference in the vertical velocity (Fig. 5c) is very similar to that of the radial velocity with the upward motion (red) in front of the blade being stronger for the spherical particles whilst the downward flow (blue) behind the blade is almost unchanged. When all the components are combined to give the speed, the spherical particles have increased speeds in front of the blade (more red), very similar motion behind the blade (also red) and reduced activity in the bed between the piles (now dark blue).

The shape and speed of the surface material does not sufficiently characterise the behaviour of the bed-blade interaction. It is important to also understand the internal flow within the bed. To do this a cylindrical grid co-moving with the blade is super-imposed over the flow and the particle velocities are averaged onto the nodes of the grid. This creates average steady state representation of the flow field that can be visualised in various ways. Figure 6 shows velocity arrows rendered at the nodes of this grid. The length of each arrow is proportional to the average speed at that location and the arrow is oriented in the direction of the velocity. The flow is more localized around the blade for the spherical
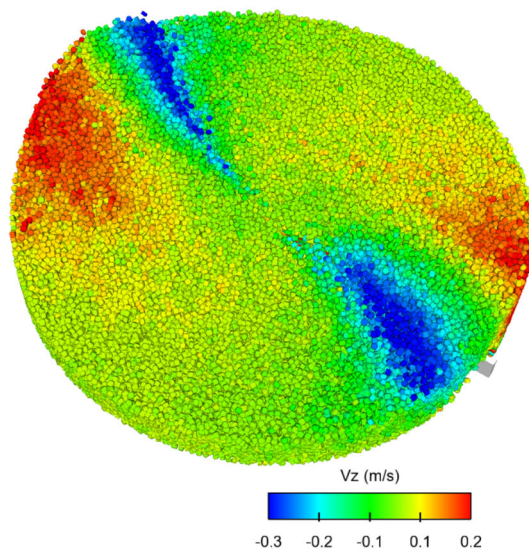
(a) Radial Velocity
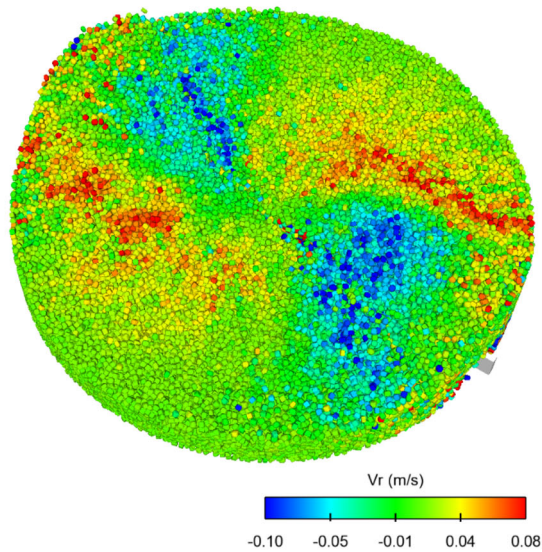
(b) Azimuthal Velocity
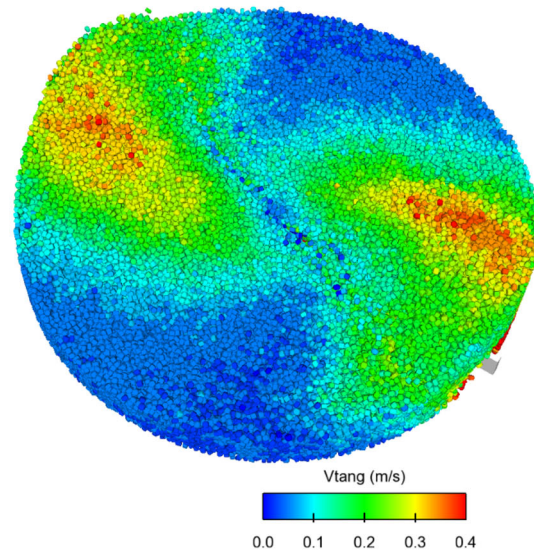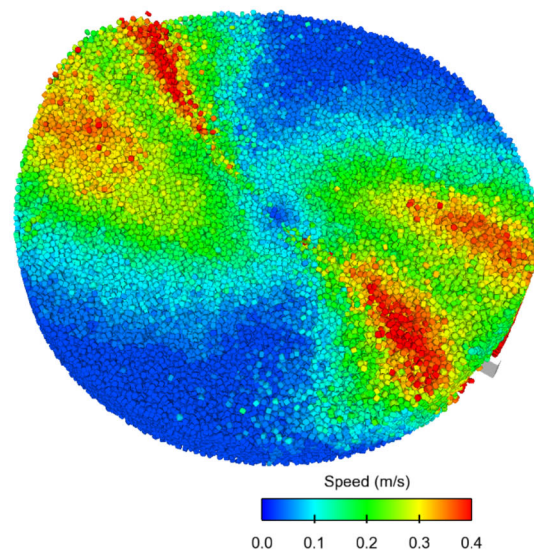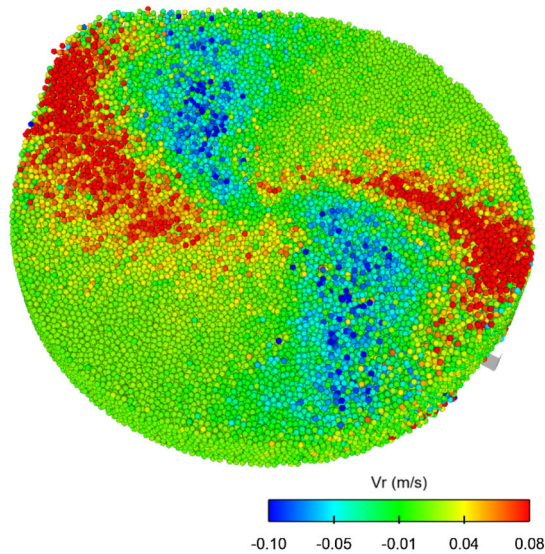
(c) Vertical Velocity

(d) Speed

Fig. 4 Particle velocities of the quasi-steady bed for the super-quadric mixture for, **a** radial velocity; **b** tangential or azimuthal velocity; **c** vertical velocity, and **d** speed

particles (Fig. 6b). The highest speeds are observed for the small region directly in front of the blade where particles are forced to move at the blade tip speed of 0.7 m/s. Particles in advance of the blade flow upwards towards the free surface and then more quickly down the free surface. Particles behind the blade flow downwards into the void created by the forward motion of the blade. Particles also flow over the blade throughout the depth of the pile above the blade. There is little motion in the bed away from the blade. For the non-round particles (Fig. 6a) the flow near the blade is very similar with the same form or upward flow in advance of the blade, down-

ward flow into the space behind the blade and flow over the blade. The most important differences are the much higher speeds in the bed between the piles. Reasonable flow speeds are observed near the mixer shell around the full perimeter of the mixer. The flow on the free surface of the pile is also more erratic due to the large variability in post-collision velocities for non-round particles. There is no evidence of the recirculation zones inside the heap in front of the blade as previously identified by [49,50] and [57,58] at the lower tip speeds of 0.1–0.52 m/s that they used. Chandratilleke et al. [7] showed that such recirculation zones reduced in size with
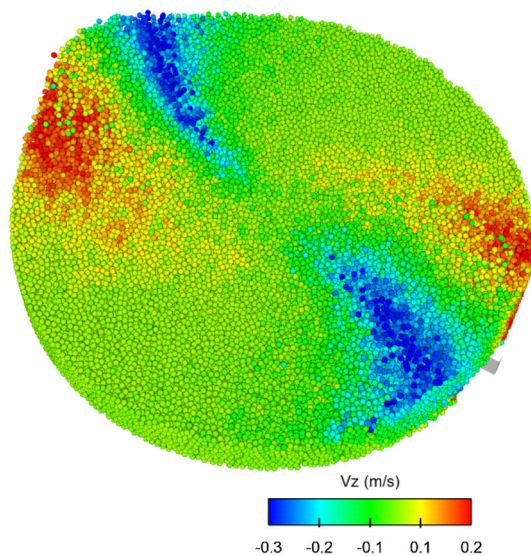
(a) Radial Velocity

(b) Azimuthal Velocity
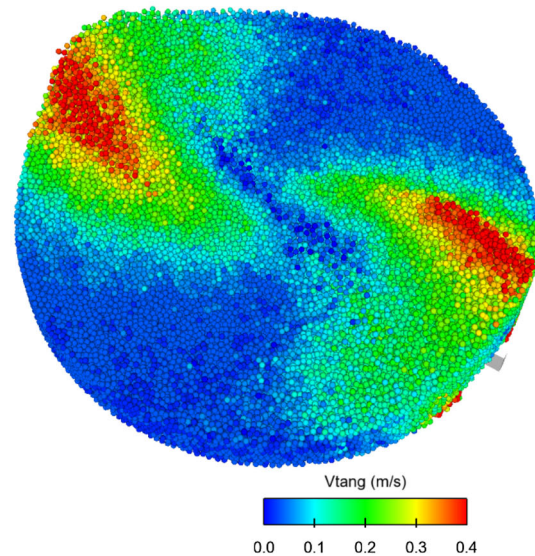
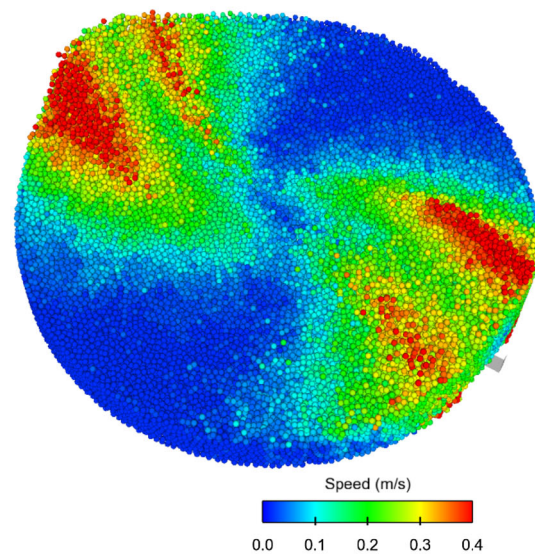**(c)** Vertical Velocity

(d) Speed

Fig. 5 Particle velocities of the quasi-steady bed for spherical particles for, **a** radial velocity; **b** tangential or azimuthal velocity; **c** vertical velocity, and **d** speed. The colour ranges are the same as for Fig. 4

increasing blade speed up to 1.3 m/s. This occurs because there is sufficient upward force transmitted to the particulates at higher speeds that they are able to flow over the blade and are no longer trapped in front of it. The circulation zones around the blade dominate the mixing that is produced by this mixer. The larger is the size of the flow region generated around he blade to the better is the configuration for mixing performance.

Figure 7 shows an isosurface of granular temperature for the two shape cases both from above and from the side in a view that is orthogonal to the blade. An isosurface encloses a

volume of the space that connects all the points with a specified value of the granular temperature. A reasonably high value of the granular temperature of 0.01 is used to show the regions in which strong velocity fluctuations occurs. Since diffusive mixing is usually considered to be dependent on the granular temperature, the regions identified here are the principle locations in which strong diffusive mixing occurs. For the spherical case, there is a larger coherent triangular region located in advance of the blade and one with equal length (along the blade) but narrower in terms of depth behind the blade. From the side on view, both of these structures are
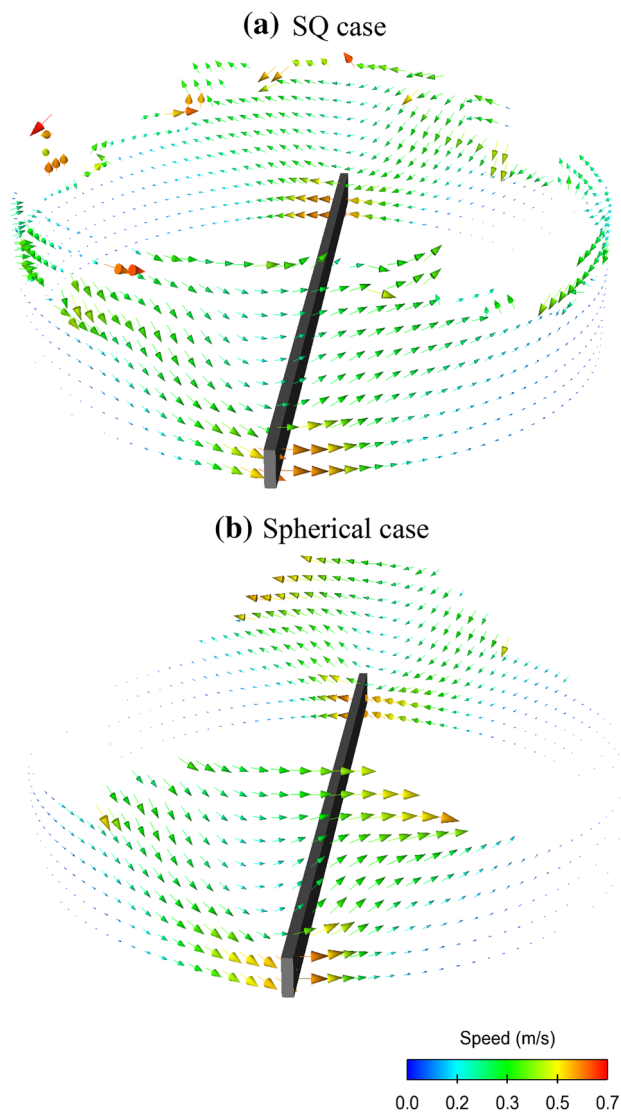
(a) SQ case

(b) Spherical case

Speed (m/s)

0.0   0.2   0.3   0.5   0.7

Fig. 6 Velocity field for **a** SQ mixture, and **b** spherical particles

predominantly at or below the top of the blade extending modestly above with increasing radius out to the mixer shell. There is a second large structure located above this that corresponds to the surface regions of the pile. It starts in advance of the blade and follows the mixer shell. Once the blade is passed then it broadens. This corresponds to avalanching free surface material flowing from the top of the pile down and inwards away from the blade. For the super-quadric case, the granular temperature is noisier. At and below the blade there are similar large scale regions both in front of and behind the blade. The one in front of the blade is smaller while the one behind is shorter in the radial direction but larger in the azimuthal direction. The remaining noisier structure is all located at or near the free surface and corresponds also to the free surface avalanche flow driven by the blade and it co-moving pile structure. An important difference is that these structures extend much further in the azimuthal

direction around the inner surface of the mixer shell. The reason for this is the nature of the interaction of the flowing bed with the stationary mixer shell. Spherical particles adjacent to the wall are able to roll which does not generate much granular temperature [13] whereas non-round particles cannot roll easily tend to slide more and rolling motion generates quite strong granular temperature which is required to dilate the bed and provide the space needed for the elongated particles to rotate. Overall, the spherical particle case has higher granular temperature and larger areas of higher granular temperature which extend radially further towards the center of the mixer. This suggests that the spherical particles will have greater diffusive mixing and that this diffusive mixing will occur over a larger range of radii within the mixer.

Figure 8 shows the dilation and compaction for the two shape cases. The blue isosurfaces indicate regions where the bed is dilating rapidly whilst red surfaces are ones indicating regions undergoing strong compaction. There is a region of strong compaction in advance of the outer half of the blades which can be seen clearly in both views for both types of particle shape. The region is larger for the spherical particles which are less interlocked and less able to resist the compression forces produced by the blade pushing into the bed. There is a second larger compaction zone. For the spherical particles, this starts at the mixer shell slightly in advance of the blade and then occupies an arc behind the blade ending just past the center of the mixer. The side view shows that this is a surface region that follows the free surface from the highest bed location in the pile above the blade adjacent to the mixer shell down to the lowest point in the center of the mixer just above the top of the blade. This is the broad zone where the particles that are flowing over the blade and avalanching down the rear surface of the pile that co-moves with the blade settle and compact into the denser bed. For the super-quadric particles this region also exists but is much smaller and is located only at smaller radii well away from the mixer shell. This occurs because the angle of repose for the pile is larger and the bed depth is shallower in the middle of the mixer so the particles do not slow and compact until further down the slope than occurred for the spheres. A second effect is that the larger granular temperature near the mixer shell for the non-round particles continues to keep the bed more dilated and so the extent of compaction near the shell is reduced. It is worth noting that the strong compaction zone extends all the way to the floor of the mixer and in fact widens with proximity to the floor, whereas the spherical particle compaction was restricted to the surface layers. The blue isosurface shows regions of strong dilation. There is one large region around each side of the blade. The basic structure is similar for both particle types. For the spherical particles the region is a bit smaller extending towards the shell only at the front of the pile in front of the blade. There is also strong

dilation in the surface layers above and just behind the blade
as a result of the flow of particles over the blade within the
piles. In contrast, for the super-quadric particles the dilation
region is larger and extends to larger radii over much of the
region in front of the blade. The dilated surface layers above
and just behind the blade at smaller radii are also larger. The
dilation is clearly enhanced by the particles being non-round
and is a consequence of shear in the bed requiring dilation of
the bed in order for the particles to rotate. The shape of the
particles has a very clear and visible impact on the amount
and distribution of both the compaction and dilation of the

bed (both of which spatially affect the ability of the bed to
mix)

Figure 9 shows the shear behaviour for the two shape
cases. Regions of medium and high shear are shown by the
blue and red isosurfaces respectively. The regions are struc-
turally similar for both shape cases but are mildly larger for
the super-quadric shape. Very high shear occurs in a thin
layer along the front and back of the blade. For the spher-
ical particles, this extends to the floor near the middle of
the mixer but its depth decreases with increasing radius to
give a triangular shape red region in the side on view. There

Fig. 9 Isosurfaces of shear rate with values 5 and 10 s^{-1}(given by the *blue* and *red* colours for (*left*) SQ mixture, and (*right*) spherical particles and shown from: **a** above, **b** and **c** the side in an orientation that is orthogonal to the blade
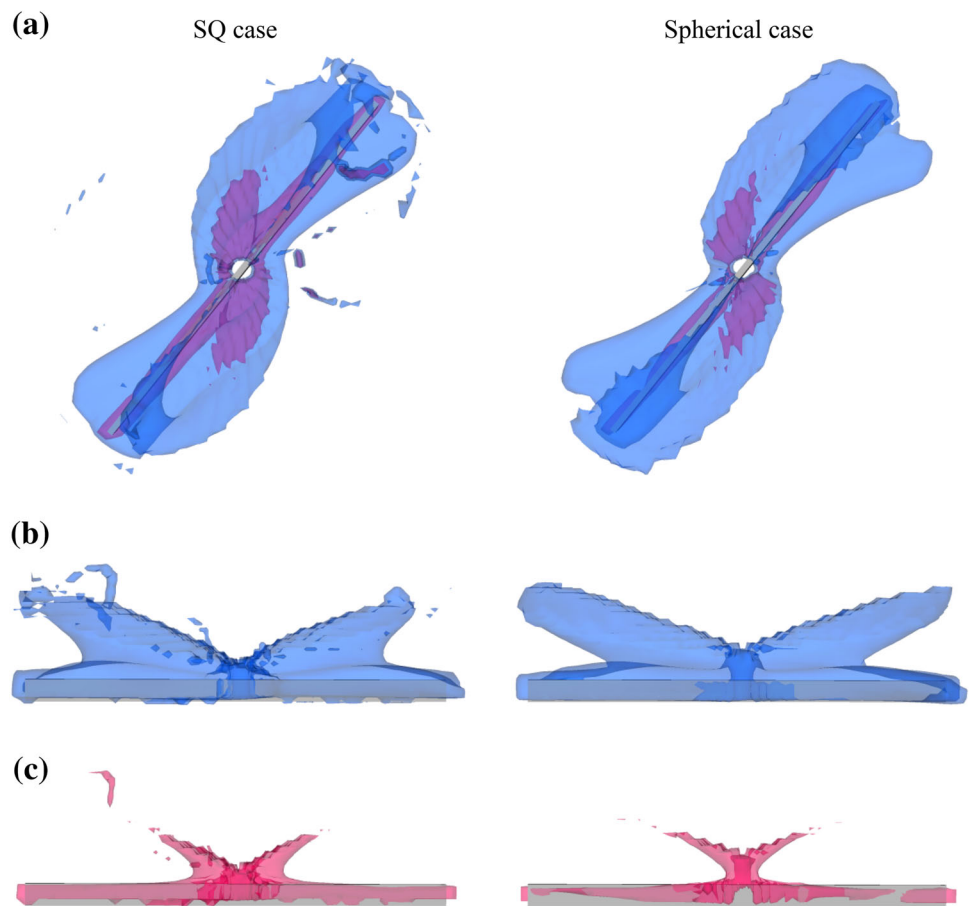

is also a narrow region of high shear in the surface layers near the center of the mixer. In contrast, for the non-round particles the high shear extends to the floor along the full length of the blade and the central surface region is substantially wider (as seen in the side view). The free surface shear structure (when viewed from above) extends into the bed at around a 30 degree angle behind the blade. The size of the high shear (red) region viewed from above is also noticeably larger for the non-round particles. The medium shear level (blue) isosurface has a lobe in front of the blade and a larger one behind the blade. It extends closer to the shell for the spherical case but is wider in the direction transverse to the blade for the non-round particles. There is a reasonable degree of similarity in the volume and shape of the medium shear rate regions. This suggests that the convective component of mixing is likely to be quite similar for the two particle shape cases with moderately better mixing in the center of the mixer for the non-round particles.

4.2 Mixing comparison

To begin the comparison of the relative mixing performance we consider the deformation of one quadrant of the bed. This

is shown in Fig. 10, for the spherical and non-spherical cases with the particles coloured by height. The spherical case has previously been shown in [16]. For the spherical case (left column of Fig. 10), particles are pushed up into a heap in front of the approaching blade which sweeps through the bed. Particles near the floor of the mixer (blue) remain there as a distinct layer but are stretched in the azimuthal direction. Particles that are higher up (green) flow over the blade, (as demonstrated by the mean flow pattern shown in Fig. 6), and are then deposited on the top of the bed behind the moving impeller (as shown in Fig. 10b). In between the stretched layers of blue and green particles is another layer formed by particles from the other quadrants which are also stretched in the azimuthal direction but which are not visible. Particles from different quadrants therefore form almost horizontal layers as a result of the shearing by the blade. The number of such layers in the vertical direction increases with the number of blade passes with these layers becoming correspondingly thinner. This stretching is a critical aspect of the mixing behaviour of this mixer design. Figure 10c shows the surface bed layer and the layer near the floor for the single quadrant after 1.5 revolutions, at which time the visible particles stretched around the entire circumference of the mixer.

Fig. 10 Progressive deformation of a single quadrant for **a** spherical particles, and **b** super-quadric mixture. The *rows* are at three successive times. The particles are coloured by height to identify the layers of the flow


(a) Spherical case

(b) SQ case
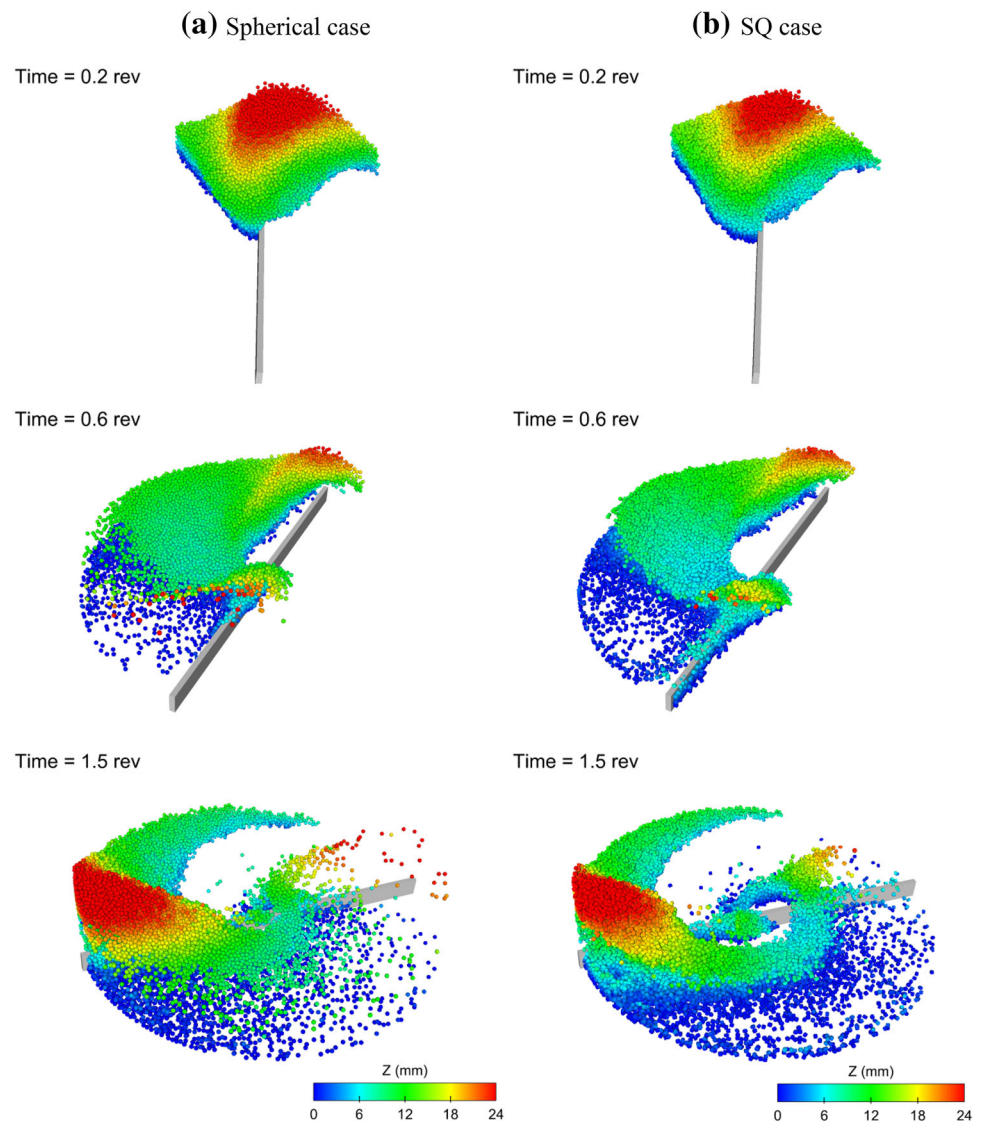
Near the surface is a fast moving pile (coloured red) above each end of the blade. They predominantly rotate with the blade and undergo relatively little mixing.

The corresponding state of the deformation of the initial quadrant is shown for super-quadric particles in the right column of Fig. 10. The structure is quite similar, particularly in the early stages when the amount of deformation is still quite small. At 0.2 rev, the pile of super-quadric particles above the blade is slightly lower and the pile is slightly more rounded, but the differences are of no practical significance. After 0.6 rev, still subtle but larger quantitative differences have emerged. The main green mass is slightly closer the blade at the top and the rear surface is more coherent. The upper surface which was almost completely green for the spherical particles now has green particles only in the outer half of the mixer while the particles closer to the center are lights blue with some mid-blue particles just visible. This is

the result of the weaker diffusive mixing that occurs for the non-round particles. The bottom layer of dark blue particles is denser and more coherent indicating that a larger fraction of the particles near the flow of the mixer are left behind the faster moving surface layers. There is also a larger amount of material on the other side of the blade both at the bottom of the blade (particles coloured dark blue) and near the surface of the bed (light blue to green), particularly near the center of the mixer. At 1.5 revs, the most visible difference is that the super-quadric particles form a very clear and coherent spiral that extends for more than one circuit of the mixer ending at the center of the mixer. This is substantially the consequence of the high central shear observed in the middle of the mixer as shown in Fig. 9. For the spherical particles, the central shear is weaker so there is less wind up of the spiral and the stronger diffusive mixing erases the weaker convective structure. The stronger diffusion also leads to lower coherency of

Fig. 11 Mixing of the four particle quadrants for **a** SQ particles, and **b** spherical particles. The *rows* show the mixing state after 1, 2 and 4 blade revolutions


(a) SQ case

(b) Spherical case
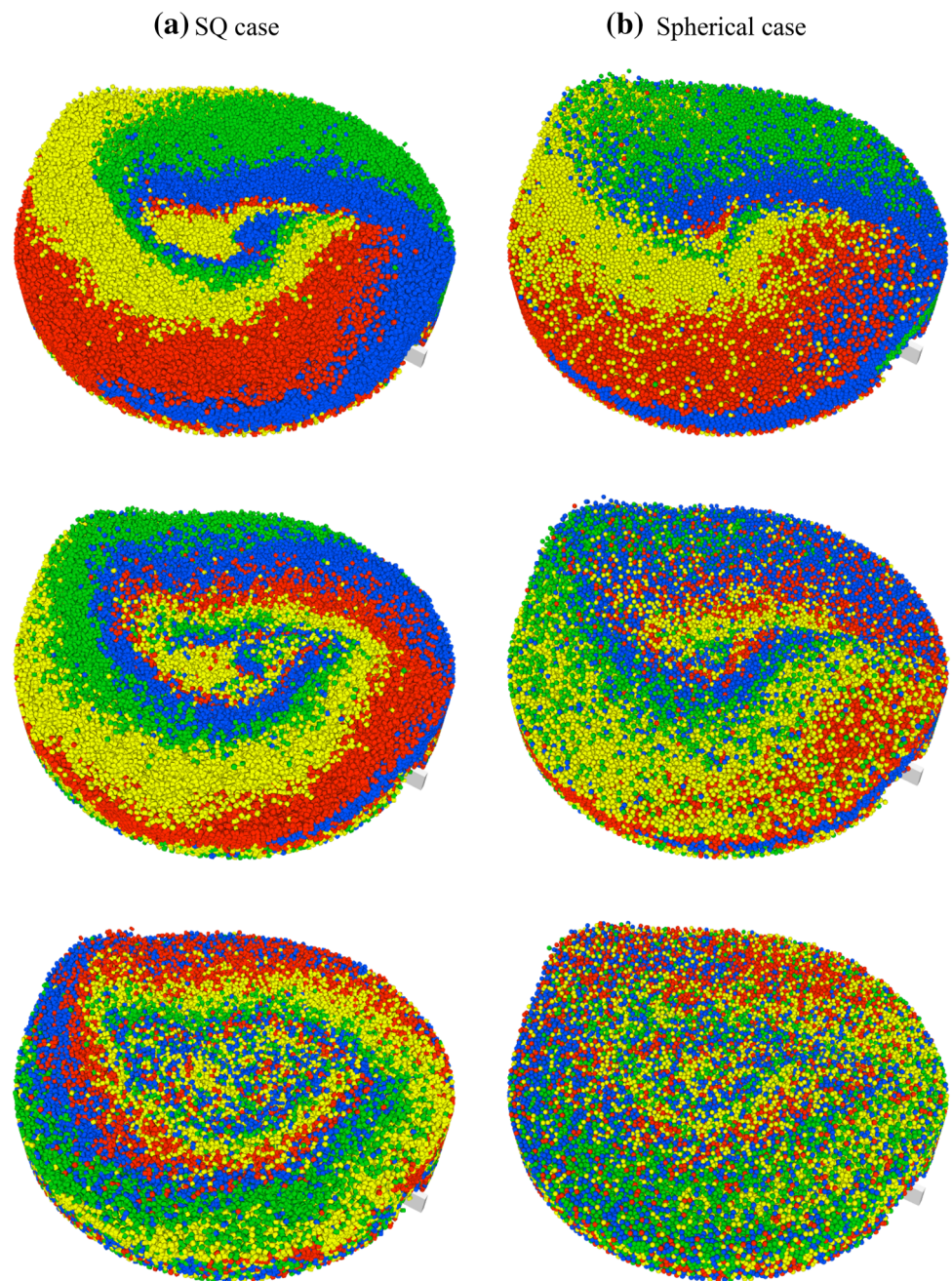
the surface regions of the deformed particle mass. The denser and more coherent dark blue bottom layer is also quite clearly visible. Overall, Fig. 10 shows that the basic flow pattern and the mixing fundamentals are not much affected by the shape of the particles, but the amount of diffusive mixing is clearly lower for the non-round material which strongly affects the coherency of the structures created.

Mixing can be visualised by colouring the particles in different banded arrangements as shown in Fig. 3. Figures 11, 12, 13 show the comparative mixing in the azimuthal, radial and vertical directions by showing the evolution of

quadrants, annular bands and horizontal strata for the two particle shape cases. In each case, we can identify the nature of the mixing in that direction and the relative changes produced by the particles being non-round.

Figure 11 shows the progression of mixing of quadrants for the non-round mixture case and the spherical case. The stretching motion generated by the rotating blade generates a spiral pattern as the outer part of each quadrant moves faster than the inner parts. The number of turns in the spiral increases linearly with the number of blade rotations and the width of each spiral arm decreases as its length extends.

Fig. 12 Mixing of the four equal volume annular regions for **a** SQ particles, and **b** spheres. The *rows* show the mixing state after 1, 2 and 4 blade revolutions

(a) SQ case

(b) Spherical case
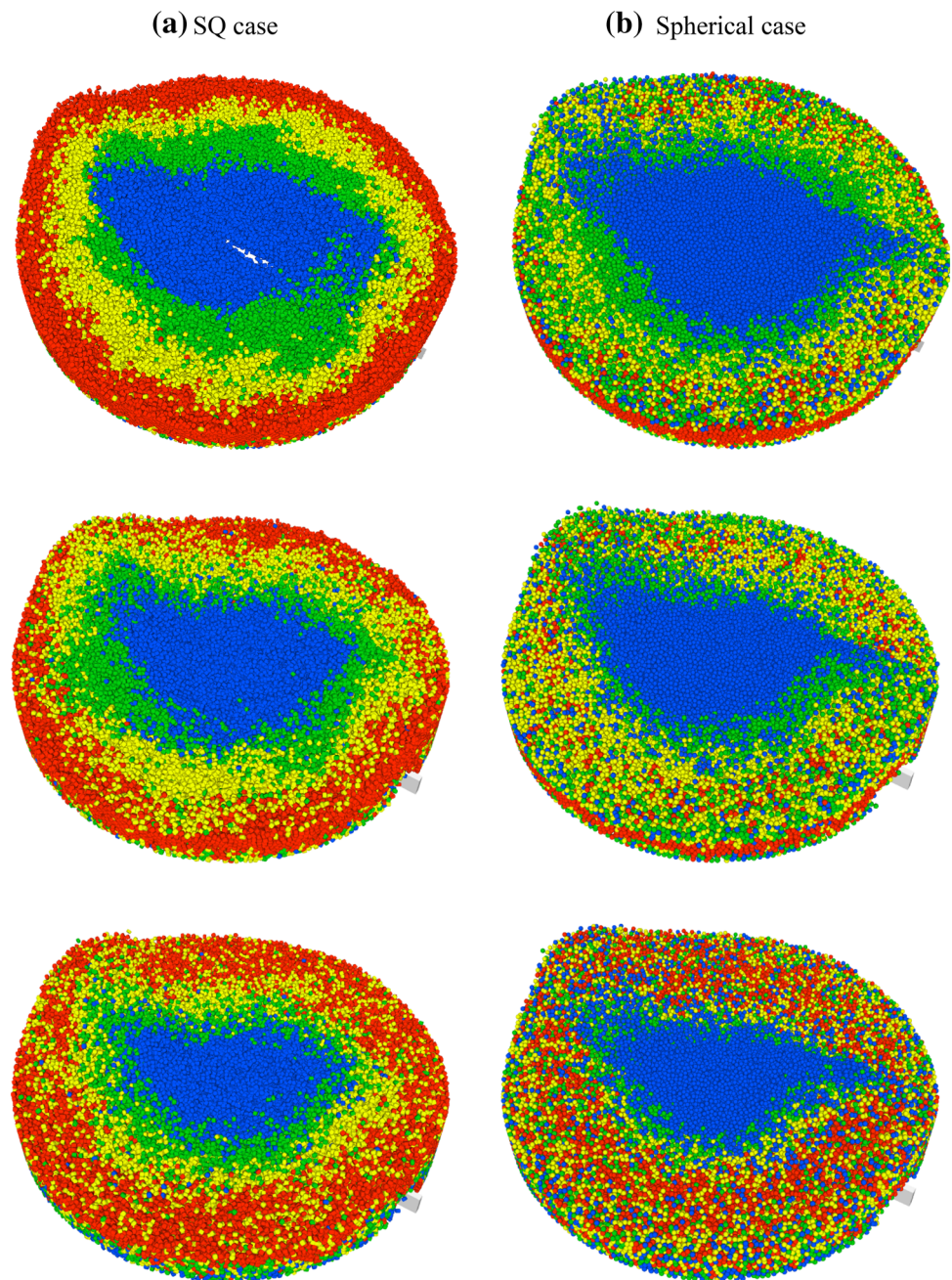
At 2 blade revolutions the spiral is nearly 720° in angular length. A relatively poorly mixed layer is visible near the floor which is a consequence of the lower layer (which was shown in Fig. 10 as blue) adjacent to the floor which has little radial or vertical motion and so is only stretched azimuthally but at a slower rate than for the material above. At 1 revolution, the super-quadric bed has significant azimuthal stretching but only weak diffusive mixing across the interfaces between the colours. At 2 revolutions, the stretching has doubled and the coloured bands are becoming reasonably narrow. Moderate diffusive mixing across the interfaces can now be seen. At 4 revolutions, the accumulated dif-

fusion is becoming quite large and the colour interfaces are no longer distinct. The colour bands can no longer be resolved in the inner half of the mixer where the stretching has caused the bands to become much thinner than the average diffusive displacement. In the outer half of the mixer, the diffusion distance is comparable to the thickness of the colour bands which are still resolvable as concentrations of colour but without any clear interfaces separating them since the diffusion has now blurred structures of this scale but not eliminated them entirely. This pattern continues and the colour regions can soon no longer be resolved after 8 revolutions.
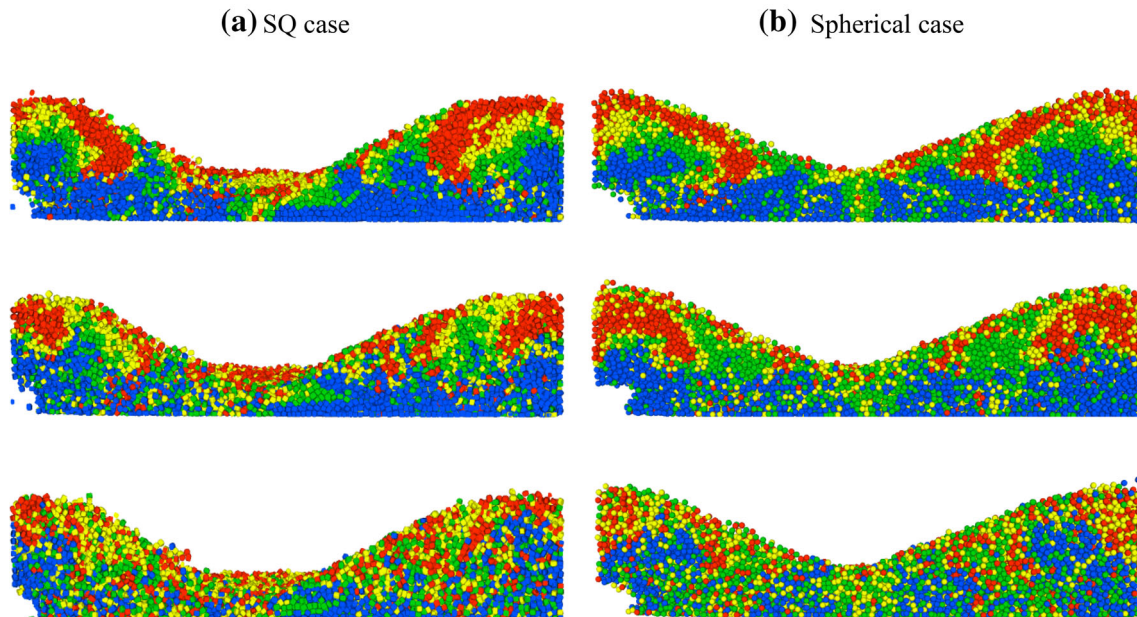
(a) SQ case   **(b)** Spherical case

Fig. 13 Mixing of the four equal volume horizontal strata for **a** SQ particles, and **b** spheres. The *rows* show the mixing state after 1, 2 and 4 blade revolutions

The spherical particle distribution demonstrates similar qualitative behaviour with the stretching of the spiral arms resulting from the azimuthal stretching of the quadrants. However, the higher particle flowability leads to much more local diffusive mixing of the colours across the colour interfaces. So for example there is significant intermixing of the yellow with red and the green and the dark blue after 2 revolutions when compared to the state for the SQ particles. The spiral pattern is less resolvable in the center partially due to the weaker central shear (as shown in Fig. 9) but also due to the stronger diffusion (as shown by the larger granular temperature in Fig. 7). Overall, the convective behaviour is similar except in the middle but the diffusive mixing is stronger for the spherical particles. By 4 revolutions, the material is already reasonably mixed with only some large scale variations in the colour distributions.

Figure 12 shows the progression of mixing of the annular bands for the non-round mixture case and the spherical case. There are some important differences in the radial transport with shape. The SQ annuli remain fairly coherent with limited diffusion between regions after one blade revolution (Fig. 12a). In contrast, the spherical bed already is visually very different with almost all of the red material no longer visible. This is the result of the three dimensional circulatory flow around the blade and the greater flowability of the spherical material which allows the top (red) layer to sink into the bed and to be covered by green and yellow particles flowing outward from smaller radii. After 2 revolutions (Fig. 12b), the bed of non-round particles retains its annular structure but with increased diffusion between colour bands. This behav-

iour continues, and by 4 revolutions there has been significant outward diffusion of yellow into red. The mixing of the green and blue is entirely diffusive with equal inward and outward mixing of these bands. The radial mixing is strongly dominated by diffusion with only a weak convective component at larger radii. The radial mixing is significantly slower than the azimuthal mixing—which should be expected since the dominant stretching component of the flow generated by the blade is in the azimuthal direction. The radial components of the flow are relatively weak so the convective component of mixing is relatively much weaker than the diffusion (which is controlled by the granular temperature which is isotropic). For the spherical material, the diffusive mixing is faster (which is consistent with the larger regions of high granular temperature in Fig. 7). The coupling of the radial and vertical flow for this case sees substantial amounts of red material return to the surface by 4 revolutions but this is very well mixed with the yellow and reasonably mixed with the green. The blue central core of material remains poorly mixed (as it was for the super-quadric material). This poor central mixing is a consequence of the piles created by the blade only reaching half way to the center of the mixing. The radial motion of the bed generated by the blade motion occurs as a three dimensional circulation in front of, behind and above the blade in the outer half of bed (as shown in Fig. 6). In the inner regions, where the bed is of comparable or lower height to the blade then flow over the blade ceases and flow in front of and behind the blade is more a rigid body rotation with the blade without any circulatory component. The radial mixing is the weakest direction of the mixing and
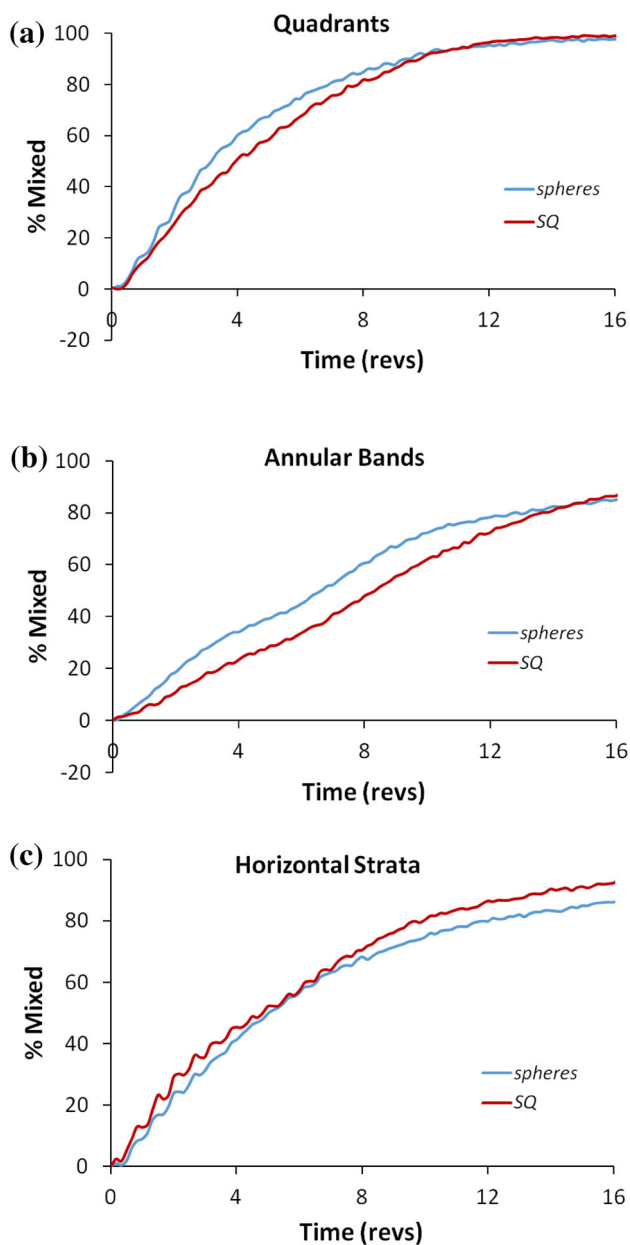
(a)

Quadrants

(b)

Annular Bands

(c)

Horizontal Strata

Fig. 14 Mixing performance as a function of the number of blade revolutions quantified for each mixing regime: **a** quadrants (azimuthal mixing); **b** annuli (radial mixing); and **c** horizontal strata (vertical mixing) for spherical particles and a super-quadric mixture

the mixing in the inner half is poor—which limits the overall mixing timescale and the ultimate limit of the mixing efficiency.

Figure 13 shows the progression of mixing of horizontal strata in the vertical direction for the non-round mixture case and the spherical case. The view is horizontal and shows a slice from the middle of the bed close to the blade. The effect of the circulation pattern in the piles on either side can be clearly observed. After only 1 revolution, the upper levels of the non-round particle bed (red, yellow and green) have

undergone quite strong convective mixing which breaks up these strata into several distinct pieces which are interspersed. The diffusive mixing at this time is still small as shown by the relatively coherent interfaces between the colour regions. The bottom blue layer, whilst perturbed is still substantially unmixed. At 2 revolutions, the colour groups have been further subdivided by the convective component of the mixing driven by the blade induced circulations in the bed. The diffusive mixing has increased with the interfaces being less distinct. The blue bottom layer has become somewhat intermixed with parts of the other layers, but to a much smaller extent than the other ones. At 4 revolutions, the non-blue strata look quite mixed and even the blue layer is becoming increasingly mixed with the rest of the bed, For the spherical particles, the behaviour is qualitatively very similar. An importance difference is the subduction of the red (initially top strata) below the free surface. Even at 1 revolution there is a thin layer of yellow and green covering the main red strata, which is the same behaviour as was observed in the disappearance of the red outer annulus from the free surface in Fig. 12. For the spherical material the radial outflow quickly covers the material that was at the free surface of the piles. The vertical mixing is not obviously any faster for the spherical particles than for the non-round ones. This is consistent with the lack of difference in the vertical distributions of granular temperature (Fig. 7) and shear rate (Fig. 9) which are measures of the diffusive and convective mixing. So the particle shape does not appear to much affect the vertical component of the flow or of the mixing.

The mixing in the azimuthal direction is the strongest due to the very strong stretching that the blade induces in this direction. This is predominantly convective in nature. The vertical mixing is also relatively quick and effective. However, the material near the bottom of the mixer (below the top of the blade) is mixed more slowly than the material above. The radial mixing is much slower. There is a weak convective component near the ends of the blade due to the circulation in the piles pushed by the blade. There is little radial convective transport in the inner half of the mixing. Radial mixing is predominantly diffusive in nature and this also decreases with radius due to decreasing granular temperature with radius (as shown in Fig. 7). In general the interfaces between colour regions are more coherent for the non-round material than for the spherical one reflecting the lower rate of diffusive mixing for this non-round material. This arises from the greater flowability of the spherical particles which have a weaker microstructure and which are less able to resist shear stress resulting in more diffusion. The mixing times for the non-round particles are therefore longer than for the spherical particles. This is also consistent with the behaviour recently reported by [15] for mixing in a ploughshare mixer.

Figure 14 shows the time variation of the mixing measure for each of the directions of mixing for the non-round mix-

Fig. 15 Mixing state for quadrants after 0.8 blade revolutions for SQ particles blockiness of **a** 3.0, **b** 4.0, **c** 5.0, and **d** 6.0
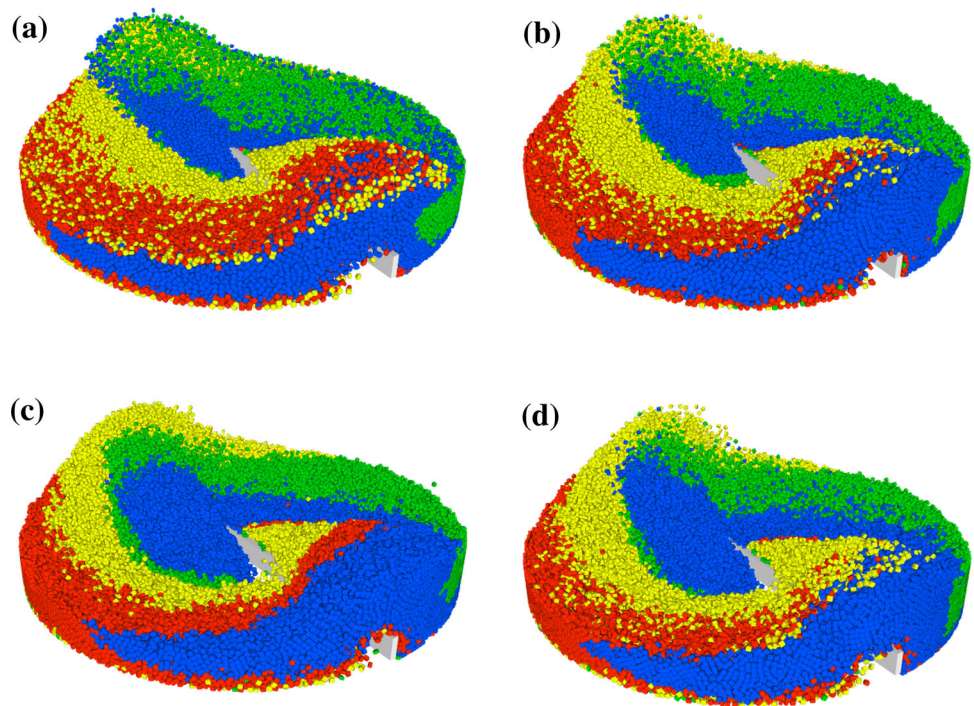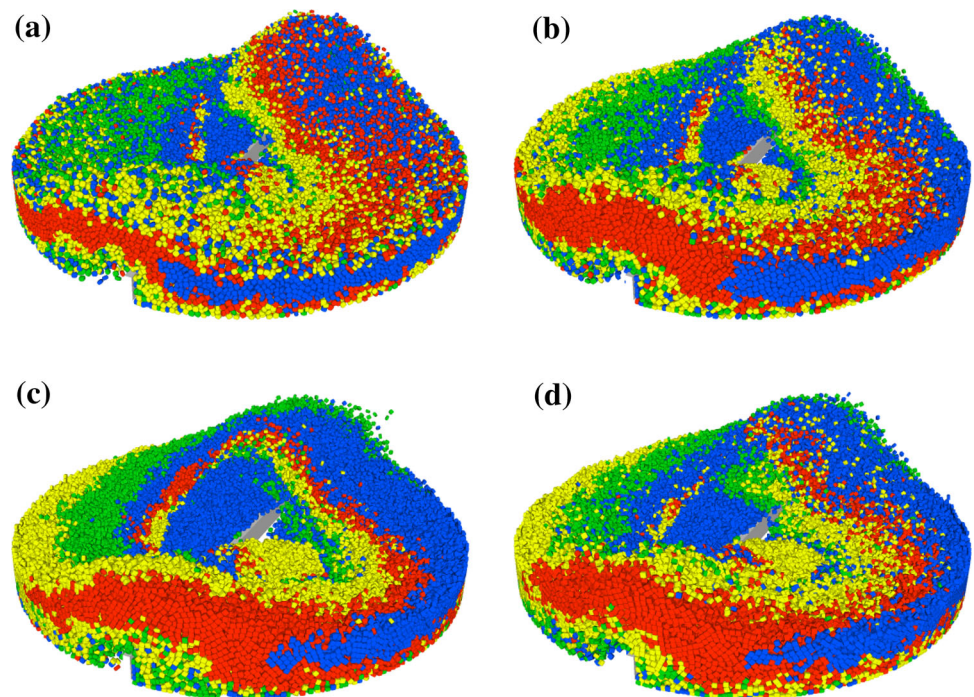
(a) **(b)**
(c) **(d)**

Fig. 16 Mixing state for quadrants after 1.7 blade revolutions for SQ particles blockiness of **a** 3.0, **b** 4.0, **c** 5.0, and **d** 6.0

(a) **(b)**
(c) **(d)**

ture and spherical particle cases. In all cases, the percentage mixed theoretically starts from zero. The mixing measure increases rapidly over the first several revolutions and then progressively decreases as it asymptotically approaches its limiting mixed state. The mixing data is shown for the first 16 revolutions. The mixing of the quadrants, which is broadly controlled by the azimuthal stretching of the particle bed driven by the rotation of the blade, is very similar for the two types of particle shape. The mixing is most different at around 4 revolutions with the spherical case being 60 % compared to 51 % for the non-spherical one. At 10 revolutions, these have increased to 92 % for both shapes of particles. The curves approach each other and both beds are fully mixed at 14 revolutions which corresponds to a mixing time of 8.4

Fig. 17 Mixing state for quadrants after 3.3 blade revolutions for SQ particles with blockiness of **a** 3.0, **b** 4.0, **c** 5.0, and **d** 6.0
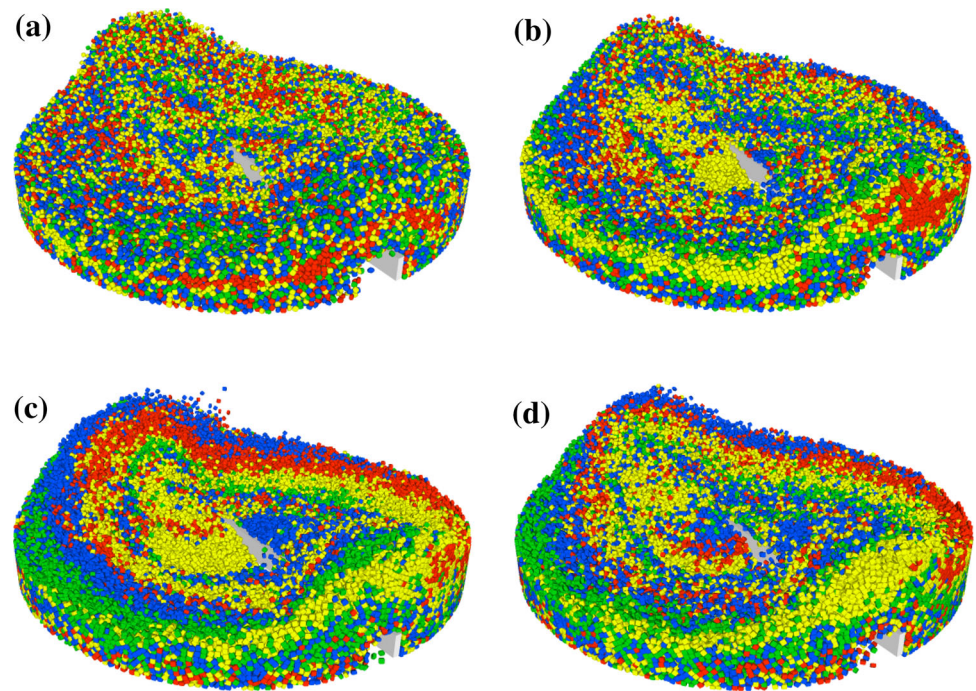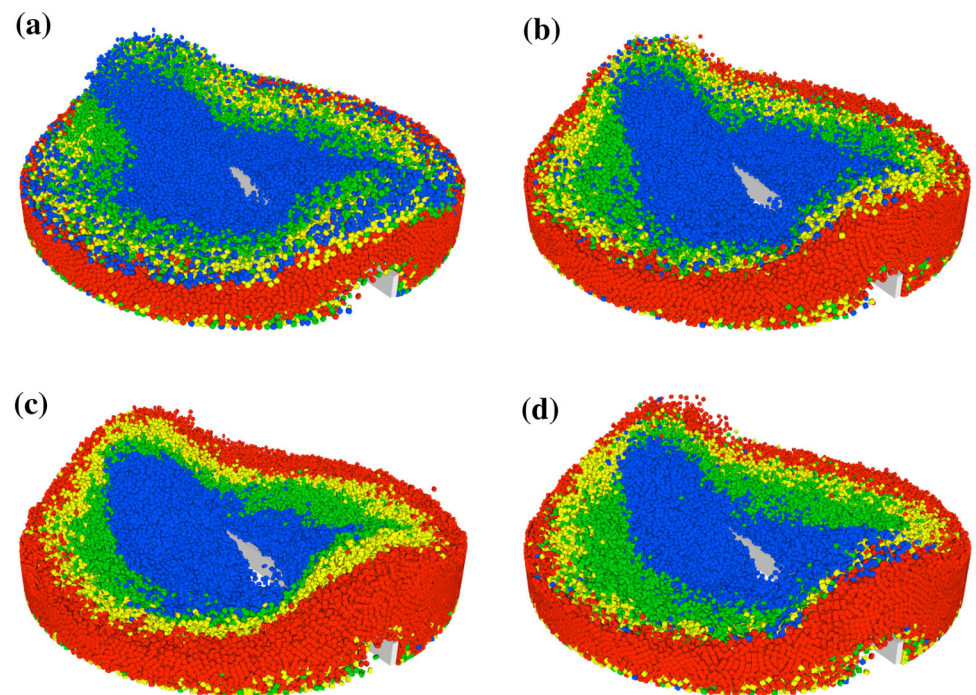

Fig. 18 Mixing state for annular regions after 0.8 blade revolutions for SQ particles blockiness of **a** 3.0, **b** 4.0, **c** 5.0, and **d** 6.0

s. Zhou et al. [57] estimated total mixing for a homogenous mixture (initially coloured into two halves rather than quadrants) would take about 7 revolutions in a larger mixing vessel with a blade tip speed of 0.25 m/s (19 rpm). This corresponds to a total mixing time of 22.1 s. This is consistent with the predictions of [7] where they demonstrated that mixing time improves greatly with blade speed but mixing performance per revolution degrades with speed up to about 0.65 m/s tip

speed. So that it takes more revolutions to reach a perfect mixture (as observed here).

The radial mixing (as indicated by the annular bands and shown in Fig. 14b) is controlled by the radial flow within the piles (as shown in Figs. 5 and 6) and is much slower than for the azimuthal (quadrant) mixing. For this mixing direction there is a strong particle shape effect with a substantially slow rate of mixing for the non-round

Fig. 19 Mixing state for annular regions after 1.7 blade revolutions for SQ particles with blockiness of **a** 3.0, **b** 4.0, **c** 5.0, and **d** 6.0
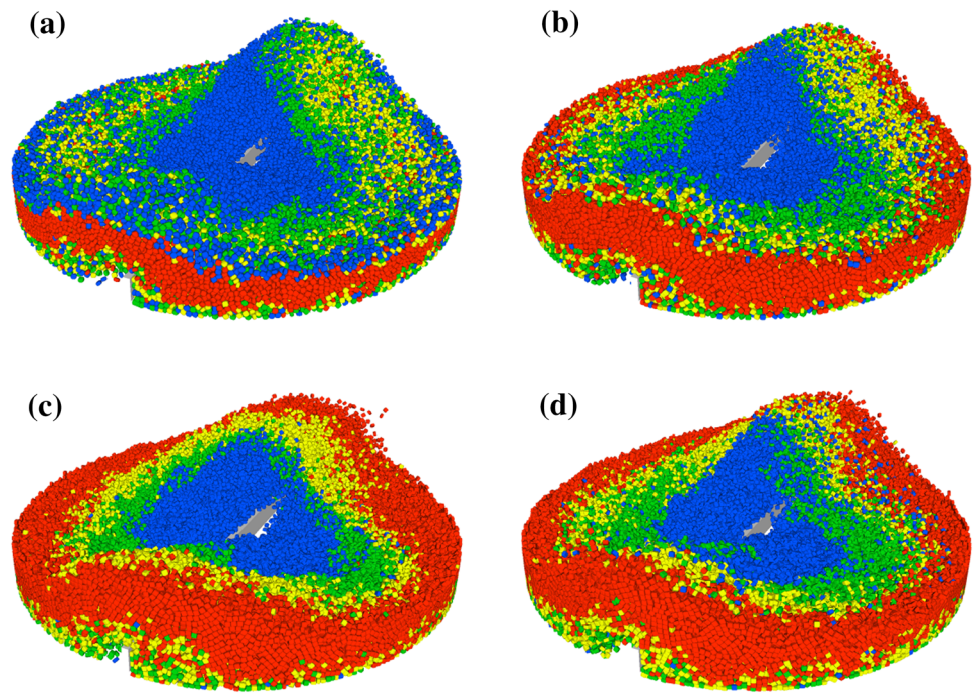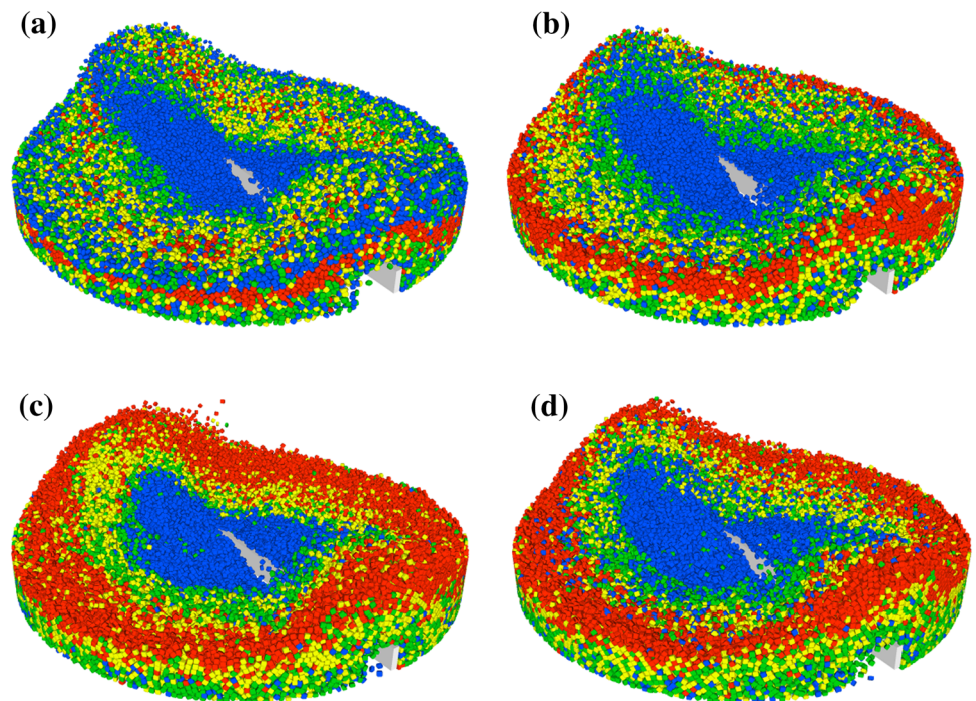

Fig. 20 Mixing state for annular regions after 3.3 blade revolutions for SQ particles with blockiness of **a** 3.0, **b** 4.0, **c** 5.0, and **d** 6.0

material. After 10 revolutions the mixing degree is only 62 % for the non-round particles compared to 72 % for the spherical ones. This is a consequence of weaker radial velocities and of the reduced diffusive mixing observed earlier (as indicated by the smaller regions of high granular temperature for the non-round particles as shown in Fig. 7).

The vertical mixing behaviour (Fig. 14c) is quite similar for the two shapes of material with the super-quadric case being slightly stronger than the spherical over the full mixing period but only by a small amount. This is consistent with the relative invariance in mixing observed when comparing the horizontal strata evolution in Fig. 13. The mixing percentage reaches 75 % for the spherical particles after 10

Fig. 21 Mixing state for horizontal strata after 0.8 blade revolutions for SQ particles with blockiness of **a** 3.0, **b** 4.0, **c** 5.0, and **d** 6.0
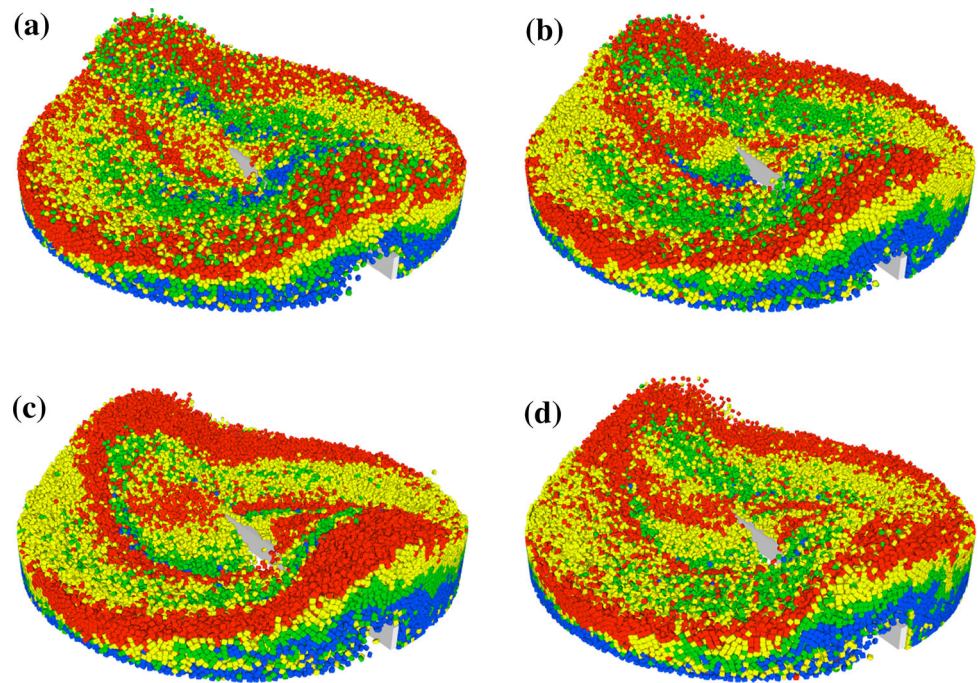
revolutions compared to 80 % for the non-round ones. The bed is nearly fully mixed at 16 revolutions. The remaining less mixed material is near the floor of the mixer and reflects the difficulty that this machine has in fully mixing particles that are well below the top of the blade and which tend to be pushed around the bottom of the mixer in a nearly rigid body rotation with the blade rather than moving relative to the blade and becoming mixed.

From these comparisons it is clear that the shape of the particles reasonably affects the rate of mixing, although to different degrees in each of the three directions. In the following sections we explore the functional dependence of the mixing on the different shape attributes—namely the blockiness and aspect ratios of the particles.

5 Effect of particle blockiness on mixing

One of the key shape attributes of a particle is its blockiness—which is an indication of whether it is angular with edges and corners or rounded. For super-quadric shaped particles this is controlled by the power m Eq. (3). Here we use oblate super-quadric particles with one aspect ratio fixed at 0.7 and the other fixed at 1.0 and vary the blockiness from $m = 3$ (nearly ellipsoidal) to 6 (brick like), as shown in Fig. 2. These aspect ratios were chosen as they are representative of the middle of the range of these shape attributes. All the particles in each simulation are the same size and shape and only the blockiness varies between cases shown.

Figures 15, 16, 17 show the degree of mixing of quadrants after 0.8, 1.7 and 3.3 revolutions respectively. Each shows the

state for blockiness values $m = 3, 4, 5$ and 6. At 0.8 revolutions the $m = 5$ case shows little diffusive mixing with quite sharp interfaces between the stretched quadrants. There is slightly more diffusion visible (as indicated by the decreasing coherency of the interfaces) for $m = 6$ and then $m = 4$. The $m = 3$ case shows the strongest diffusion. For the more blocky material, the yellow quadrant flows over the top of the pile giving a thick yellow layer over the green on the pile over the blade at the back of the mixer. As the particles become more rounded, less yellow material flows over the blade and the pile is increasingly dominated by the green quadrant. This indicates that the blockiness is also influencing the degree of convective mixing. At 1.7 revolutions (Fig. 16) similar behaviours are visible. The $m = 5$ case still demonstrates only weak diffusion with the diffusive mixing increasing for both higher and lower blockiness values. Significant amounts of diffusion are visible for $m = 3$. The influence of the blockiness on the convective mixing is most visible in the increasing dominance of the top surface of the back pile on the blade of the green quadrant particles. By 3.3 s, the $m = 3$ and 4 cases show significant mixing. The higher blockiness cases show significant stretching of the quadrants (creating convective mixing) but have much more limited diffusion. For the $m = 5$ case, the stretched quadrants remain reasonably coherent.

Figures 18, 19, 20 show the degree of mixing of annular bands after 0.8. 1.7 and 3.3 revolutions respectively for the four different blockiness levels. We recall that the spherical case ($m = 3$) in Fig. 12 had quite different behaviour to the non-round mixture with the red outer band being rapidly submerged under particles from the other bands. In Fig. 18, we

see the same behavior for the more rounded $m = 3$ case. As m increases, this behaviour decreases with a substantial amount of the red band remaining at the surface for $m = 4$ and very little radial movement of any of the bands for higher m. This behaviour continues over time. At 1.7 revs, the red band remains submerged with a thick layer of blue and green above and a thin mixed layer below. As m increases, the outermost region is increasingly dominated by the red annular band. The amount of diffusive mixing of the annuli also appears to decrease with blockiness. By 3.3 revolutions, much of the top of the bed is well mixed for $m = 3$ except for the central core of blue material. This does not mix well for any of the shapes. The $m = 5$ has the most coherency in the bands, indicating that the diffusive mixing of the annular bands is also a minima for this shape. For $m = 4$, the red band has been pushed to the outer edge of the bed and is largely submerged. For more blocky particles, the red band remains on the surface near its original location. This indicates that the radial components of the circulation in the piles around the blade are strongly influenced by the blockiness of the particles with rounded particles being much more mobile and circulating freely. The speed and extent of the radial component of the circulation decreases quickly as the particles become more angular and can better interlock.

Figure 21 shows the degree of mixing of horizontal strata after 0.8 revolutions for the four different blockiness levels. The stretching and degree of convective mixing is generally similar for all four blockiness levels, but there is a modest increase in the length of the stretched structures created with increasing blockiness. The other difference between these blockiness cases is in the degree of diffusive mixing which is minimal for $m = 5$ and increases for both more and less blocky material and which is quite strong for $m = 3$ whose colour interfaces are already reasonably blurred. These behaviours continue with increasing blade rotations which are not shown.

The behaviour of the diffusive mixing for the different blockiness levels is very similar for each of the three mixing directions. This should be expected as the diffusive mixing is controlled by the granular temperature which is an isotropic quantity—so the diffusion should be direction independent as is observed to be the case in these simulations.

The convective mixing is affected differently by the blockiness change depending on the direction. The basic azimuthal stretching and the vertical component of the circulation are broadly unaffected by the blockiness. The radial motion within the piles created by the blade is quite strongly affected by the blockiness. This affects the convective mixing of the quadrants near the blade and strongly influences the radial mixing in the outer radial half of the mixer. The radial motion is strongest for the most round particles and decreases as the particles become more blocky.
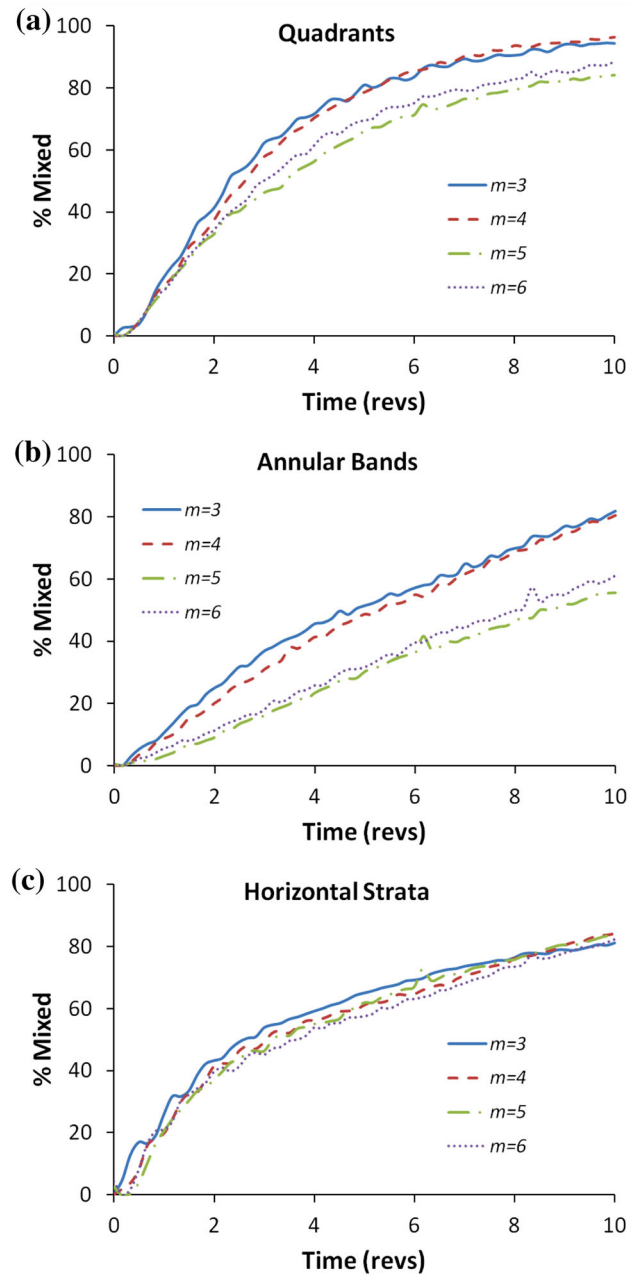

Fig. 22 Effect of particle blockiness on the time variation of the mixing for each direction, **a** quadrants, **b** annular bands, and **c** horizontal strata

Figure 22 shows the time variation of the quantitative mixing measure and how this changes with the blockiness for each of the mixing directions. For the quadrants, (Fig. 22a), the best mixing occurs for the more rounded particles with the $m = 5$ particles having the slowest mixing and the $m = 6$ ones being moderately faster. This is consistent with the behaviours observed in the mixing pictures (Figs. 15, 16, 17). For the annular bands, (Fig. 22b), the mixing is less good for all the shapes than it was for the quadrants. This is consistent with the earlier comparison of the spherical and

Fig. 23 Mixing state for quadrants after 3.3 blade revolutions for SQ particles with aspect ratios: **a** 0.5, **b** 0.7, **c** 0.85, and **d** 1.0
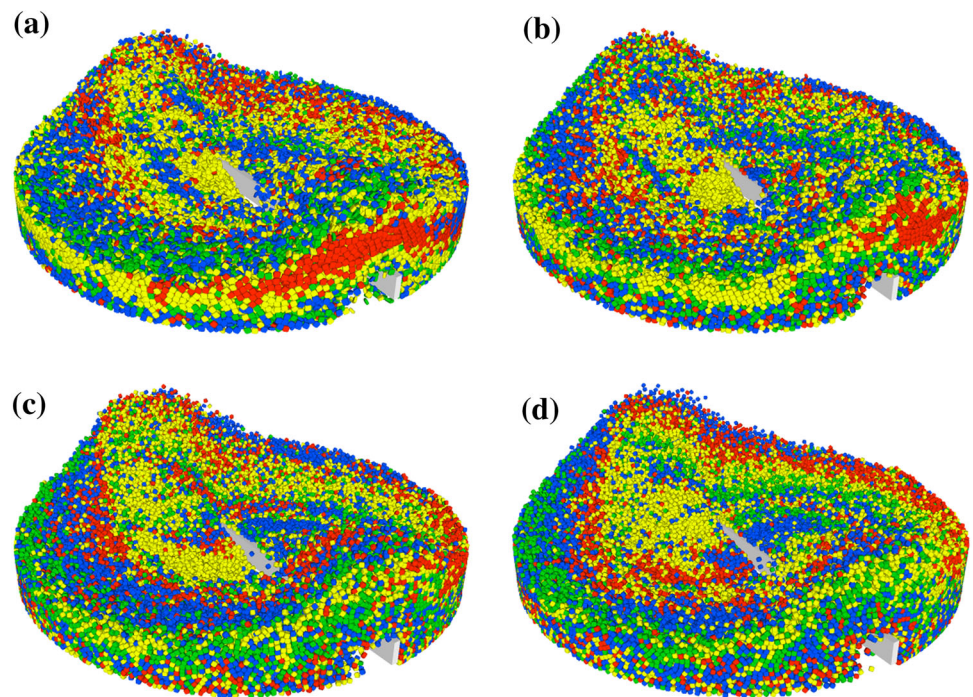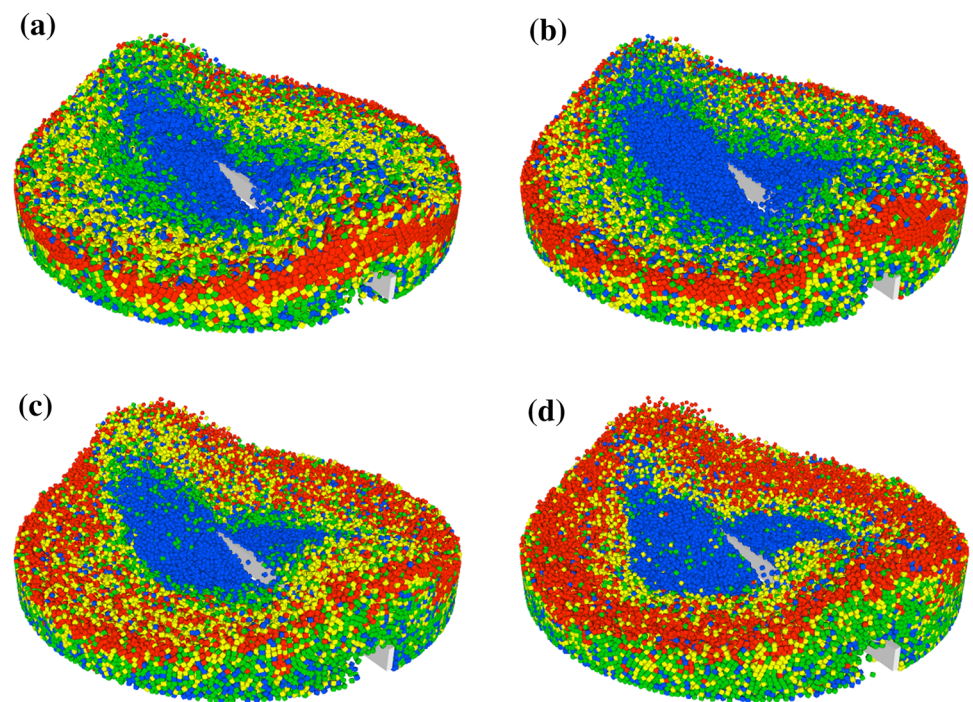

Fig. 24 Mixing state for annular regions after 3.3 blade revolutions for SQ particles with aspect ratios: **a** 0.5, **b** 0.7, **c** 0.85, and **d** 1.0

non-round mixture cases. Consistent with the flow pictures (Figs. 18, 19, 20) the annular mixing is much stronger for the rounder particles with the $m = 5$ case being the slowest. For the horizontal strata, Fig. 22c shows that all four sets of particles have very similar mixing behaviour. Better diffusive mixing for more rounded particles is balanced by slightly better convective mixing in the vertical direction for the more blocky particles. The invariance of the overall mixing with blockiness is consistent with small visible differences in the flow coloured by strata (Fig. 21).

6 Effect of aspect ratio on mixing

The other key shape attributes of a particle are its aspect ratios—which are an indication of how elongated and flattened the particle is. For super-quadric shaped particles this is controlled by ratios c/a and b/a of the semi-major axes in Eq. (3). Here we use super-quadric particles with blockiness $m = 4$ and with one aspect ratio fixed at 1.0 while the other is varied from 0.5 to 1.0. This gives a series of increasingly flat or oblate particles with a squarish front face and decreasing depth with increasing minor axis aspect ratio. Some examples are shown in Fig. 2. The $m = 4$ value was chosen as it is representative of the middle of the range of blockiness values considered in the previous section. All the particles in each of these simulations are the same size and shape and only the minor axis aspect ratio varies between cases.

Figures 23 shows the mixing state of the bed after 3.3 revs for aspect ratio $\beta = 0.5$, 0.7, 0.85 and 1.0 when the particles are initially coloured in quadrants. Broadly, the amount of mixing is quite similar for all the shapes. One aspect of the convective mixing that is aspect ratio dependent is the distance over which each quadrant is stretched. This process is shown in Fig. 10. As the aspect ratio decreases the length from the blade to the rear of the particles in a quadrant increases steadily. The residual effect of this can be seen in the existence of a coherent band of red for $\beta = 0.5$ in Fig. 23. The extent of diffusive mixing is very similar for all four shapes. Figure 26a shows the progress of mixing of the quadrants as given by the quantitative measure. This is very similar in all cases with the largest differences occurring around 6 revolutions with the weakest mixing being for the smallest aspect ratio.

Figure 24 shows the mixing state of the bed after 3.3 revs for aspect ratio $\beta = 0.5$, 0.7, 0.85 and 1.0 when the particles are initially coloured in annular bands. For equi-axed particles (aspect ratios near unity) the outer red band remains on the surface. This is very similar to the behaviour observed for the non-round particle mixture (see Fig. 20). As the aspect ratio decreases the red band is increasingly submerged below the outward moving green and yellow bands. The structure of the current particles is very similar to the one shown in Fig. 20 for $m = 4$ with both aspect ratios of 0.7. For smaller aspect ratio values the red band is fully submerged below the surface in the same way as was observed for more rounded particles. These changes in bed structure do not obviously lead to improved convective mixing. The rate of diffusion, as indicated by the rate at which the interfaces lose coherence, is similar for all the aspect ratios. Figure 26b shows the progress of mixing of the annular bands as given by the quantitative measure. As for earlier cases, this direction of mixing is much slower than for the other directions reflecting the relatively poor radial mixing of the central blue region which is not mixed particularly well for any of the particle shapes. There is a moderate degree of sensitivity in the rate of mixing but the relationship to the aspect ratio is not monotonic—with the $\beta = 0.7$ case having the fastest mixing while $\beta = 0.5$ has the slowest with the more equi-axed particles in between.

Figure 25 shows the mixing state of the bed after 3.3 revs for aspect ratio $\beta = 0.5$, 0.7, 0.85 and 1.0 when the particles are initially coloured into horizontal strata. The bed structure

Fig. 25 Mixing state for horizontal strata after 3.3 blade revolutions for SQ particles with aspect ratios: **a** 0.5, **b** 0.7, **c** 0.85, and **d** 1.0
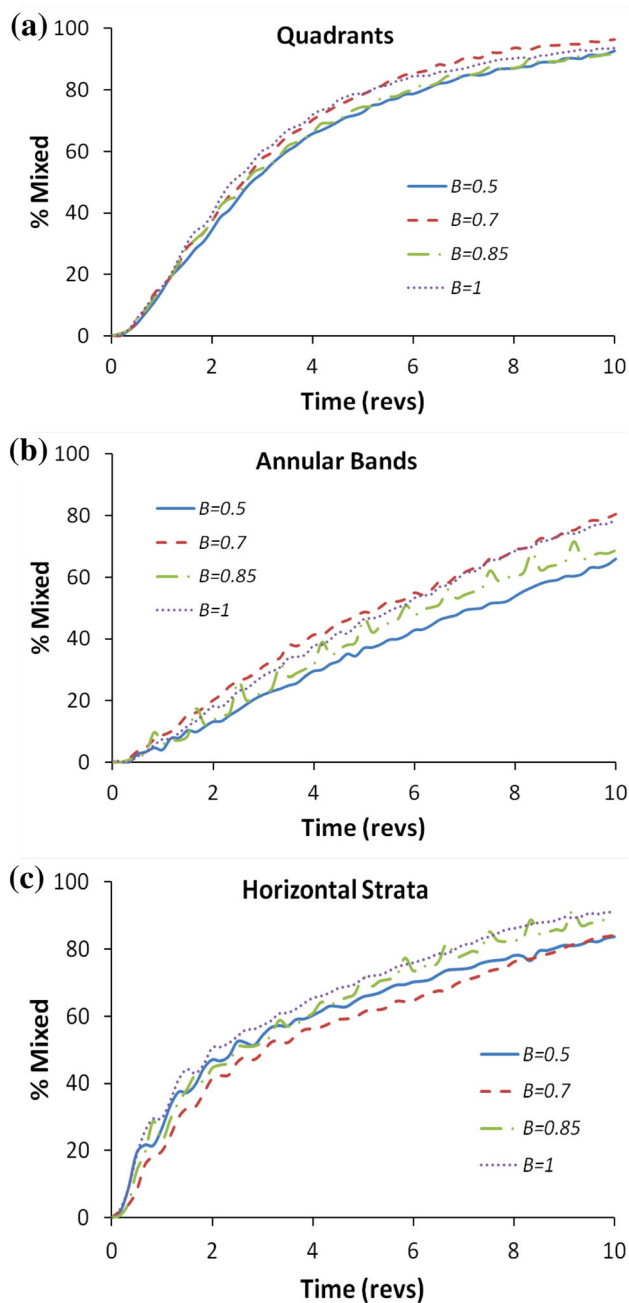
a)

b)

c)

d)

(a)

(b)

(c)
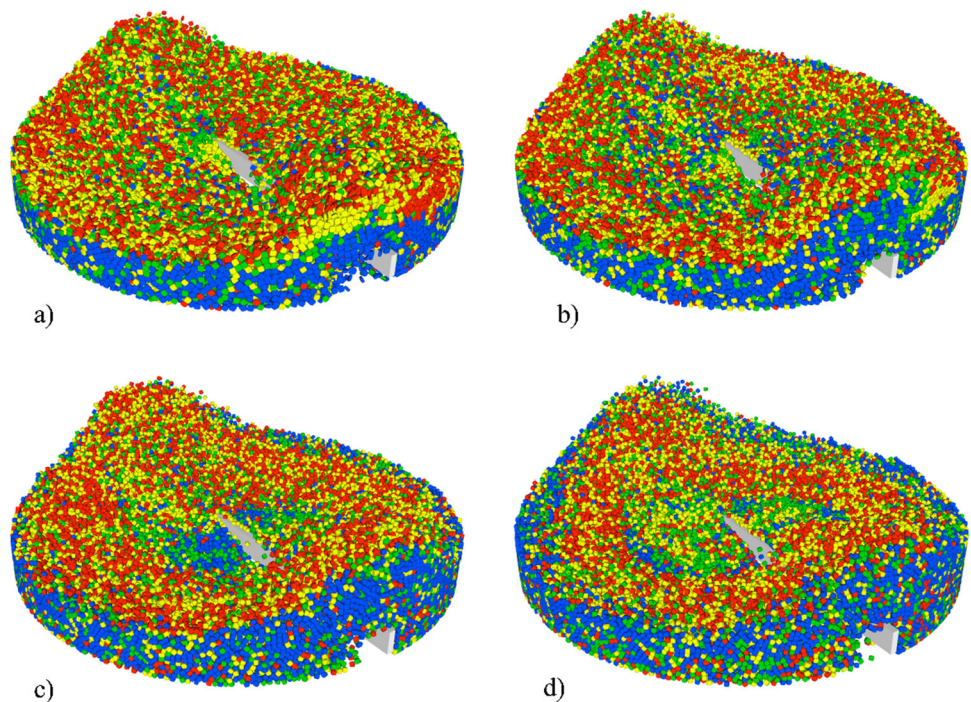
Fig. 26 Effect of particle aspect ratio on the time variation of the mixing for each direction, **a** quadrants, **b** annular bands, and **c** horizontal strata

is very similar for all aspect ratios. The only meaningful variation is a tendency for the blue dominated strata to have risen to the surface at the outside of the mixer for the equiaxed particles. With decreasing aspect ratio the mixture of red, green and yellow increasingly dominates the surface. Otherwise the vertical mixing is very similar for all cases. Figure 26c shows the progress of mixing of the strata as given by the quantitative measure. This is identical for all aspect ratios up to 4 revolutions. After this there is some divergence

with the more equi-axed particles mixing slightly faster than the flatter (lower aspect ratio) particles.

7 Conclusion

Mixing in a high shear mixer using a central vertical blade is achieved by creating a complex three dimensional flow pattern within the granular bed. Particles close to the floor of the mixer and close to the blade are pushed in front of the blade. Higher material flows upward and over the blade, generating a pile whose peak trails the blade by around $2°–3°$ and then falls into the space behind. This is accompanied by radial flow both outwards and back inwards in different regions relative to the blade location. Material near the top of the impeller blade moves more quickly than material both above and below which means that the strain rate is strongly dependent on height. This leads to very strong stretching behaviour in the azimuthal direction with material at different heights moving substantially different distances. The vertical and radial flow within the piles that move with the blade create the folding component that is required for mixing.

Mixing has both convective and diffusive components. Calculation of the strain rate tensor allows the identification of spatial regions where the flow dilates and compacts and where the shear strain rate is high. Compaction and dilation behaviour are strongly affected by particle shape since shear generates rotation which requires dilation of the bed. The shear strain rate is an indicator of the convective nature of the flow and provides insight into where convective mixing is strong. In the high shear mixer, high shear rates are found along the front and back surfaces of the blade and in a small surface region in the center of the mixer. Moderate shear is found in a dual lobed structure that is broadly centered on the blade with contributions both in front of and behind the blade. This region is found to be only slightly sensitive to the particle shape indicating that the convective mixing is relatively independent of shape, except in the middle of the mixer. The particle bed compacts in a region directly in front of the blade and at the bottom of the avalanching zone at the rear of the piles driven by the blade. The size and shape of the compaction zone at the back of the blade is strongly dependent on the particle shape. The bed dilates in a large region in front of the blade where strong flow requires dilation of the bed. This is found to be particle shape dependent with increased dilation for non-round particles. Diffusive mixing intensity can be related to the magnitude of the velocity fluctuations in the flow which is indicated by the granular temperature. This shows that strong diffusive mixing occurs over a larger volume of the mixer for the spherical particles.

Particle shape affects both the nature of the flow generated by the blade and the mixing behaviour. Spherical particle shape leads to higher flow speeds within the piles around the

blade but lower speeds in the bed further from the blade. So there is greater localization of the flow near the blade for spherical particles which shear more easily and so the blade disturbance is transmitted less effectively and less of the bed is agitated at any time. For spherical particles the granular temperature is increased leading to greater diffusive mixing.

Colouring particles in quadrants, annular bands and horizontal strata is an effective way of visualizing the progress and location of mixing within the bed and allows the mixing to be quantified in the azimuthal, radial and vertical directions. Convective mixing in the azimuthal direction is relatively similar for round and non-round particles. Radial mixing is found to be much slower than the azimuthal mixing with a large central core of the bed that is slow to mix with the outer regions. This occurs because the piles, in which the radial flow occurs, only extend half way to the center of the mixer and the bed depth at smaller radii is comparable to or lower than the bed height so flow over the blade is not possible. Radial mixing is even slower for non-round particles than for spherical since the radial outflow within the piles is much stronger for spherical particles. In contrast, mixing in the vertical is very similar regardless of shape. The diffusive mixing rate is similar for all the directions since this is isotropic and driven by the granular temperature. This is higher for spherical particles because of their greater flowability.

A parametric study was used to assess the impact of the blockiness on the flow and mixing. The best azimuthal mixing occurs for the more rounded particles with the $m = 5$ super-quadric particles having the slowest mixing while the more blocky $m = 6$ particles mix moderately faster. The radial mixing is less good for all the shapes than it was for the azimuthal direction. It is much stronger for the rounder particles with the $m = 5$ case again being the slowest. Better diffusive mixing which occurs for more rounded particles is balanced by better convective mixing in the vertical direction for the more blocky particles giving vertical mixing that is essentially the same for the full blockiness range.

A parametric study of the effect of aspect ratio variation on the mixing showed that the amount of mixing is fairly insensitive to the aspect ratio. There are some modest changes in the speed of radial outflow with decreasing aspect ratio which leads to moderately slower radial mixing. The convective mixing in the azimuthal and vertical directions varies little with aspect ratios. The amount of diffusive mixing for moderately blocky particles is also relatively invariant to aspect ratio.

In summary, from this DEM analysis, the blockiness is the shape attribute that has the strongest impact on flow and mixing. The mixing has only a weak dependence on aspect ratio. One consequence of the sensitivity of the mixing to particle shape is that in using DEM to analyse and/or design such high shear mixers, it is important to adequately char-

acterise the shapes of the particles for which the mixer is being designed. It is then critical that the DEM model use an adequate representation of these shapes in order to correctly predict the performance of the mixer.

References

1. Ai J, Chen JF, Rotter JM, Ooi JY (2011) Assessment of rolling resistance models in discrete element simulations. Powder Tech 206(3):269–282
2. Arriata PE, Duong N, Muzzio FJ, Godbole P, Lange A, Reynolds S (2006a) Characterizing mixing and lubrication in the Bohle Bin blender. Powder Tech 161:202–208
3. Arriata PE, Duong N, Muzzio FJ, Godbole P, Reynolds S (2006b) A study of the mixing and segregation mechanisms in the Bohle Tote blender via DEM simulations. Powder Tech 164:50–57
4. Barker GC (1994) Computer simulations of granular materials. In: Mehta A (ed) Granular matter: an inter-disciplinary approach. Springer, Berlin
5. Bertrand F, Leclaire LA, Levecque G (2005) DEM based models for the mixing of granular materials. Chem Eng Sci 60:2517–2531
6. Campbell CS (2006) Granular material flows-an overview. Powder Techn 162:208–229
7. Chandratilleke GR, Zhou YC, Yu AB, Bridgwater J (2010) Effect of blade speed on granular flow and mixing in a cylindrical mixer. Indus Eng Chem Res 49(11):5467–5478
8. Chaudhuri B, Mehrotra A, Muzzio FJ, Tomassone MS (2006) Cohesive effects in powder mixing in a tumbling blender. Powder Tech 165:105–114
9. Cleary PW, Metcalfe G, Liffman K (1998) How well do discrete element granular flow models capture the essentials of mixing processes? Appl Math Model 22:995–1008
10. Cleary PW, Sawley M (2002) DEM modelling of industrial granular flows: 3D case studies and the effect of particle shape on hopper discharge. Appl Math Model 26:89–111
11. Cleary PW, Metcalfe G (2002) Quantitative comparison of mixing rates between DEM and experiment in a slowly rotating cylinder. In: Proceedings of World Congress on particle technology, vol 4, 21–25 July, Sydney
12. Cleary PW (2004) Large scale industrial DEM modelling. Eng Comput 21:169–204
13. Cleary PW (2008) The effect of particle shape on simple shear flows. Powder Tech 179:144–163
14. Cleary PW (2009) Industrial particle flow modelling using DEM. Eng Comput 26:698–743
15. Cleary PW (2013) Particulate mixing in a plough share mixer using dem with realistic shaped particles. Powder Tech 248:103–120
16. Cleary PW, Sinnott MD (2008) Assessing mixing characteristics of particle-mixing and granulation devices. Particuology 6(6):419–444
17. Conway SL, Lekhal A, Khinast JG, Glasser BJ (2005) Granular flow and segregation in a four-bladed mixer. Chem Eng Sci 60(24):7091–7107
18. Debroux F, Cleary PW (2001) Characterising the angles of failure and repose of avalanching granular material using the DEM method. In: 6th World Congress of Chemical Engineering, Melbourne, Australia
19. Delaney GW, Cleary PW, Hilden M, Morrison RD (2012) Testing the validity of the spherical DEM model in simulating real granular screening processes. Chem Eng Sci 68(1):215–226
20. Ding YL, Forster RN, Seville JPK, Parker DJ (2001) Scaling relationships for rotating drums. Chem Eng Sci 56:3737–3750

21. Donzé FV, Richefeu V, Magnier SA (2009) Advances in discrete element method applied to soil, rock and concrete mechanics. Electron J Geotech Eng 44:31

22. Dubey A, Sarkar A, Ierapetritou M, Wassgren CR, Muzzio FJ (2011) Computational approaches for studying the granular dynamics of continuous blending processes, 1-DEM based methods. Macromol Materials Eng 296(3–4):290–307

23. Ferellec JF, McDowell GR (2010) A method to model realistic particle shape and inertia in DEM. Granular Matter 12(5):459–467

24. Finnie GJ, Kruyt NP, Ye M, Zeilstra C, Kuipers JAM (2005) Longitudinal and transverse mixing in rotary kilns: A discrete element method approach. Chem Eng Sci 60:4083–4091

25. Fleissner F, Gaugele T, Eberhard P (2007) Applications of the discrete element method in mechanical engineering. Multibody Syst Dyn 18(1):81–94

26. Ganesan V, Rosentrater KA, Muthukumarappan K (2008) Flowability and handling characteristics of bulk solids and powders-a review with implications for DDGS. Biosyst Eng 101(4):425–435

27. Garcia X, Latham JP, Xiang J, Harrison JP (2009) A clustered overlapping sphere algorithm to represent real particles in discrete element modelling. Geotechnique 59(9):779–784

28. Hassanpour A, Tan H, Bayly A, Gopalkrishnan P, Ng B, Ghadiri M (2011) Analysis of particle motion in a paddle mixer using Discrete Element Method (DEM). Powder Techn 206(1):189–194

29. Knight PC, Seville JPK, Wellm AB, Instone T (2001) Prediction of impeller torque in high shear powder mixers. Chem Eng Sci 56(15):4457–4471

30. Kuo HP, Knight PC, Parker DJ, Adams MJ, Seville JPK (2004) Discrete element simulations of a high-shear mixer. Adv Powder Tech 15(3):297–309

31. Kwapinska M, Saage G, Tsotsas E (2006) Mixing of particles in rotary drums: a comparison of discrete element simulations with experimental results and penetration models for thermal processes. Powder Tech 161:69–78

32. Lacey PMC (1997) The mixing of solid particles. Chem Eng Res Design 75:S49–S55

33. Laurent BFC, Cleary PW (2012) Comparative study of DEM and experimental results of flow patterns in a ploughshare mixer. Powder Tech 228:171–186

34. Lemieux M, Bertrand F, Chaouki J, Gosselin P (2007) Comparative study of the mixing of free-flowing particles in a V-blender and a bin-blender. Chem Eng Sci 62:1783–1802

35. Lemieux M, Leonard G, Doucet J, Leclaire LA, Viens F, Chaouki J, Bertrand F (2008) Large-scale numerical investigation of solids mixing in a V-blender using the discrete element method. Powder Tech 181:205–216

36. Liu PY, Yang RY, Yu AB (2013) DEM study of the transverse mixing of wet particles in rotating drums. Chem Eng Sci 86:99–107

37. Lu LS, Hsiau SS (2008) DEM simulation of particle mixing in a sheared granular flow. Particuology 6(6):445–454

38. Markauskas D, Kačianauskas R, Džiugys A, Navakas R (2010) Investigation of adequacy of multi-sphere approximation of elliptical particles for DEM simulations. Granul Matter 12(1):107–123

39. Mead SR, Cleary PW, Robinson GK (2012) Characterising the failure and repose angles of irregularly shaped three-dimensional particles using DEM. In: Proc. ninth international conference on CFD in the minerals and process industries, CSIRO, Melbourne, Australia. 10–12 Dec 2012

40. Metcalfe G, Shinbrot T, Mccarthy JJ, Ottino JM (1995) Avalanche mixing of granular solids. Nature 374:39–41

41. McCarthy JJ, Shinbrot T, Metcalfe G, Wolf JE, Ottino JM (1996) Mixing of granular materials in slowly rotated containers. AIChE J 42(12):3351–3363

42. McCarthy JJ, Khakhar DV, Ottino JM (2000) Computational studies of granular mixing. Powder Tech 109(1):72–82

43. Ottino JM, Lueptow RM (2008) On mixing and demixing. Science 319:912–913

44. Pernenkil L, Cooney CL (2006) A review on the continuous blending of powders. Chem Eng Sci 61(2):720–742

45. Radl S, Kalvoda E, Glasser BJ, Khinast JG (2010) Mixing characteristics of wet granular matter in a bladed mixer. Powder Tech 200(3):171–189

46. Remy B, Khinast JG, Glasser BJ (2009) Discrete element simulation of free flowing grains in a four-bladed mixer. AIChE J 55(8):2035–2048

47. Sarkar A, Wassgren C (2010) Continuous blending of cohesive Granular material. Chem Eng Sci 65(21):5687–5698

48. Sato Y, Nakamura H, Watano S (2008) Numerical analysis of agitation torque and particle motion in a high shear mixer. Powder Tech 186(2):130–136

49. Stewart RL, Bridgewater J, Parker DJ (2001a) Granular flow over a flat-bladed stirrer. Chem Eng Sci 56:4257–4271

50. Stewart RL, Bridgewater J, Zhou YC, Yu AB (2001b) Simulated and measured flow of granules in a bladed mixer—a detailed comparison. Chem Eng Sci 56:5457–5471

51. Sudah OS, Coffin-Beach D, Muzzio FJ (2002) Effects of blender rotational speed and discharge on the homogeneity of cohesive and free flowing mixtures. Int J Pharm 247:57–68

52. Sinnott MD, Cleary PW, Morrison RD (2011) Is media shape important for grinding performance in tower mills? Miner Eng 24:38–151

53. Terashita K, Nishimura T, Natsuyama S, Satoh M (2002) DEM simulation of mixing and segregation in high-shear mixer. J Jpn Soc Powder Powder Metal 49(7):638–645

54. Thornton C, Cummins S, Cleary PW (2013) An investigation of the comparative behaviour of alternative contact force models during inelastic collisions. Powder Tech 233:30–46

55. Weerasekara NS, Powell MS, Cleary PW, Tavares LM, Evertsson M, Morrison RD, Quist J, Carvalho RM (2013) The contribution of DEM to the science of comminution. Powder Tech 248:3–24

56. Zhang MH, Chu KW, Wei F, Yu AB (2008) A CFD-DEM study of the cluster behavior in riser and downer reactors. Powder Techn 184(2):151–165

57. Zhou YC, Yu AB, Bridgewater J (2003) Segregation of binary mixture of particles in a bladed mixer. J Chem Tech Biotechnol 78(2–3):187–193

58. Zhou YC, Yu AB, Stewart RL, Bridgewater J (2004) Microdynamic analysis of the particle flow in a cylindrical bladed mixer. Chem Eng Sci 59:1343–1364